Gonçalo da Silva Brissos Chimelas Cachola

Licenciatura em Ciências de Engenharia Biomédica

Dependence of IVIM-DWI Estimations on Acquisition Parameters

Dissertação para obtenção do Grau de Mestre em
Engenharia Biomédica

Orientador: Sónia Gonçalves, Professora Auxiliar Convidada, FM-UC
Co-orientador: Mário Forjaz Secca, Professor Associado, FCT-UNL

Júri:

Presidente: Prof. Doutora Maria Adelaide de Almeida Pedro de Jesus
Arguente: Prof. Doutora Rita Gouveia Nunes
Vogais: Prof. Doutora Sónia Isabel Domingos Marreiros Gonçalves
Prof. Doutor Mário António Basto Forjaz Secca

FACULDADE DE CIÊNCIAS E TECNOLOGIA
UNIVERSIDADE NOVA DE LISBOA

Setembro 2013

Copyright

Acknowledgements

First, I would like to thank to my supervisor Prof. Sónia Isabel Gonçalves, who offered me the great opportunity of doing my Master Thesis with her in ICNAS and gave me the best support a student could ask.

To Prof. Mário Forjaz Secca for creating the Biomedical Engineering course in our faculty, allowing us to study this subject and be a part of the future.

To Prof. Ruy Costa for all the motivational speeches he gave us in his class, inspiring us to do better and better every single day and to chase our dreams.

To all the friends who shared this journey in Biomedical Engineering on the last 5 years with me. Miriam Cabrita, Valter Fernandes, João Carmo, Rui Pimentel, Luis Alho, Eduardo Pontes, César Rodrigues, Fábio Nascimento, Tiago Oliveira, André Queirós, Alexandre Medina, João Sousa and to everyone else that I've shared this life experience that is called University. Special thanks to Miriam Cabrita, who was always there for me and kept with me in the long study nights and to Valter Fernandes who supported and advised me in all the decisions and steps I took in this journey.

To my Erasmus friends, for all the crazy trips in Italy and for letting me know a bit more of their culture, Marius Lhu, David Murphy, Ina Holl, Beatriz Romba, Laura Burgot, Rita Arrais and Kalina Kurstak and all the others that made Pisa the best city in the world.

To everyone in Coimbra, who received me in my Master Thesis experience and made a part of their family, Gil Hilário, Mário Gago, Telmo Neves, Joana Belém, Bruno Correia, José Ribeiro and all the others who showed me why Coimbra is the city of the students.

To all my old school friends who still keep in contact and were always there for me, Diogo Cardoso, André Teixeira, Pedro Cardoso, Vanessa Silva, Gonçalo Mateus, Dário Jesus, Hugo Café, Ricardo Manuel, Gonçalo Vaz, Gonçalo Ribeiro and Ricardo Dias. Special thanks to Ricardo Dias for being the brother that I never had and showing me how great a human being can be.

To the girl who listened and corrected me while I was training my presentation, Rita Real, thank you for all the patience you had and most of all, for helping me relaxing.

Special thanks to Sara Monteiro who was always present on the last two years, advising, supporting and essentially being the best friend someone could have.

Last but not least, to my family, especially to my cousin, my mother who always gave me strength to overcome everything and my father for being the best role model a son could have.

Everyone, thank you.

Resumo

A doença hepática gordurosa não alcoólica (DHGNA) é uma das doenças crónicas do fígado mais comuns no mundo ocidental. Está normalmente associada a distúrbios de saúde como a obesidade, diabetes e a hipertrigliceridemia. Actualmente a biópsia do fígado é a técnica mais utilizada para diagnosticar a DHGNA. No entanto é extremamente invasiva e está associada a uma elevada morbidade e erros de amostragem.

Intravoxel incoherent motion diffusion-weighted imaging (IVIM-DWI) consegue distinguir a difusão puramente molecular do movimento pseudo-aleatório das moléculas de água dentro dos microvasos. A IVIM-DWI tem emergido como uma alternativa possível para a identificação de alterações nos tecidos na DHGNA. No entanto, existem poucos estudos que estudem a dependência dos parâmetros IVIM-DWI dos parâmetros das sequências de aquisição.

Por forma a estudar esta dependência, dois estudos foram feitos: 1) estudo simulativo, onde estudámos a influência dos parametros de aquisição no erro e bias associados aos parâmetros IVIM-DWI; 2) Um estudo *In-Vivo* que serve de teste à viabilidade das sequências de *b-values* obtidas através do estudo simulativo.

Os resultados mostraram que o parâmetro mais afectado pelos parâmetros de aquisição é a pseudo-difusão (D*). Além disso, foi também demonstrado que quanto maior o número de *b-values* usado, melhor será a estimativa dos parâmetros IVIM-DWI. No entanto, a partir de um determinado número de *b-values* e para baixa razão sinal-ruído (SNR), o efeito do ruído nos extra *b-values* contraria o efeito de usar mais *b-values*. Também foi demonstrado que a sequência de *b-values* usada para a amostragem, influência bastante as estimativas IVIM-DWI.

Concluímos que a sequência de *b-values* convencionalmente utilizada não fornece estimativas óptimas relativamente ao IVIM-DWI. Além disso, os resultados demonstram que devem ser atribuídos pesos diferentes a cada parâmetro IVIM-DWI para obter uma melhor estimativa. Também foi observado que a influência do relaxamento T2 deveria ser tomada em conta no modelo *Intravoxel Incoherent Motion – Diffusion Weighted Image* (IVIM-DWI). Finalmente, o nosso estudo mostrou que na presença de Esteatose, o valor D* decresce significativamente enquanto que D descresce pouco. No entanto, as diferenças entre pacientes com esteatose e saudáveis é extremamente influenciada pelo número de *b-values* usados, levando a diferentes diagnósticos dependendo desse mesmo número.

Palavras-chave: doença hepatica gordurosa não alcoólica, intravoxel incoherent motion imaging, imagem por difusão, distribuição b-values.

Abstract

Nonalcoholic fatty liver disease (NAFLD) is one of the most common chronic liver conditions in the Western world. It is normally associated with health disorders such as obesity, diabetes and hypertriglyceridemia. The gold standard for the diagnosis and staging of NAFLD is liver biopsy, which is highly invasive and is associated with high morbidity and inherent sampling error.

Intravoxel incoherent motion diffusion-weighted imaging (IVIM-DWI) is able to distinguish between true molecular diffusion and the pseudo-random motion of water molecules inside micro vessels. IVIM-DWI has emerged in the recent years as a possible alternative to probe tissue changes in NAFLD. However few studies have addressed the problem of the dependence of IVIM-DWI parameters on pulse sequence parameters.

In order to study this dependence, two studies were carried-out: 1) A simulation study, where we studied the influence of acquisition parameters on the error and bias associated with IVIM-DWI parameters; 2) In-vivo study in order to test the performance of the b-value sequences derived from the simulation studies.

Results showed that the parameter which is more affected by the acquisition parameters is D*. Furthermore, it was also shown that the higher the number of b-values used to sample the data, the better the estimation of IVIM-DWI parameters is. However, after a certain number of points and for low SNRs, the effect of noise in extra b-values counteracts the effect of having more data points. It was also shown that the b-value sequence that is used to sample the data greatly influences IVIM-DWI estimations.

We concluded that the conventionally used b-value sequence does not provide optimum IVIM-DWI estimations. Furthermore, results show that different weights should be attributed to each IVIM-DWI parameter in order to obtain a better performance of the optimized b-value sequence. Also, it was seen that the influence of T2 relation effects should be accounted for in the IVIM-DWI model. Lastly, our study showed that in the presence of steatosis, the value D* significantly decreased while D only slightly decreased. However, the differences between patients with steatosis and healthy controls were extremely influenced by the number of b-values used, leading to different diagnosis depending on the number of b-values used in the acquisition.

Keywords: nonalcoholic fatty liver disease, intravoxel incoherent motion imaging, diffusion imaging, b-value distribution.

Abbreviations and Symbols

ADC	Apparent Diffusion Coefficient
CE-MRI	Contrast-Enhanced Magnetic Resonance Imaging
CHB	Chronic Hepatitis B
CHC	Chronic Hepatitis C
CT	Computed Tomography
D	Molecular Diffusion
D*	Pseudo-diffusion
DTI	Diffusion Tensor Imaging
DWI	Diffusion Weighted Imaging
EPI	Echo-Planar Imaging
ETL	Echo Train Length
fMRI	Functional Magnetic Resonance Imaging
fp	Fraction of Perfusion
HFF	Hepatic Fat Fraction
IVIM	Intravoxel Incoherent Motion
MRE	Magnetic Resonance Elastography
MRI	Magnetic Resonance Imaging
MRS	Magnetic Resonance Spectroscopy
NAFLD	Nonalcoholic fatty liver disease
NASH	Nonalcoholic Steatohepatitis
N_b	Number of b-values

PR	Perfusion Rate
RARE	Rapid Acquisition with Relaxation Enhancement
S	Signal Intensity
SE	Single-Echo
SNR	Signal-to-Noise Ratio
ss	Single-Shot
T_2	Spin-Spin Relaxation time
TE	Echo Time
EU	Ultrasound Elastography

Contents

Figure Contents

Table Contents

1. Introduction

Nonalcoholic fatty liver disease (NAFLD) is one of the most common chronic liver conditions in the Western world [1], progressively becoming a relevant health problem due to the increasing predominance of obesity in the world [2]. NAFLD is normally associated with health disorders such as obesity, diabetes and hypertriglyceridemia, and it is often coupled with increased production of hepatic enzymes [2].

NAFLD has four main stages of increasing severity: simple fatty liver, also known as Steatosis, Non-Alcoholic Steatohepatitis (NASH), Fibrosis and Cirrhosis [3]. Steatosis is the first stage of NAFLD and it is characterized by the excessive accumulation of fat inside the hepatocytes. It is a condition that is generally considered to be harmless, and though it does not normally have associated symptoms, it can be detected with blood tests. NASH is the second stage in NAFLD, being more aggressive than simple steatosis. Only a minor percentage of people [4] with steatosis develop NASH, which contrary to steatosis shows liver tissue inflammation in addition to fat accumulation. Fibrosis is characterized by a persistent inflammation of liver parenchyma, which results in the generation of fibrotic scar tissue around the liver cells and blood vessels. Cirrhosis is the most severe stage when scar tissue and liver cells start to develop, causing liver irregularities as well as a decrease in its size. The damage caused by Cirrhosis is permanent and cannot be reversed; it progresses slowly and may lead to liver failure. Being actually possible to diagnose NAFLD, an important step to take is to determine its stage, which would provide relevant information on prognosis [3].

Percutaneous liver biopsy is considered to be the gold standard for the diagnosis and staging [5] of NAFLD. However, liver biopsy is an invasive technique with potential risks [5], expensive, inherently prone to bias due to limited tissue sampling, and difficult to repeat [6]. This implies that the use of an alternative, non-invasive and reproducible technique for NAFLD diagnosis and staging is essential [5]. Imaging methods such as Transient Elastography [TE] using ultra-sound or dynamic Computed Tomography (CT) have been used as possible alternatives to liver biopsy in the diagnosis and staging of NAFLD. With TE, it is possible to quantify the elastic properties of tissues [7] and it has been used to evaluate liver stiffness [6, 7, 8]. Results show that the latter has a large correlation with the stages of liver fibrosis in patients with chronic hepatitis B or C [7, 8] (CHB, CHC). Dynamic CT in association with compartmental models has been used to quantify liver perfusion [10].

Magnetic resonance imaging (MRI) is a promising non-invasive method for the assessment of NAFLD, since it has the potential to generate multi-parametric information [6]. It can provide several modalities such as functional imaging (fMRI), spectroscopy (MRS), dynamic contrast-enhanced MRI (CE-MRI) or diffusion-weighted imaging (DWI), to name just a few. In fMRI the variations in the homogeneous magnetic field (B0) homogeneity due to variations of the concentration of deoxyhemoglobin [11] are measured. MRS is based on the

frequency variations of spins related to the chemical environment where they are inserted. It is used to non-invasively quantify the amount of several biological molecules that are involved in both pathological and non-pathological processes. In CE-MRI, a contrast agent is injected in the blood and the temporal variation of its uptake by the tissues is studied [12] using fast imaging pulse sequences whereas in DW-MRI, image contrast is sensitive to the diffusion of water molecules [13]. Recent studies [14] have shown that both CE-MRI and DWI provide potential markers for fibrosis and cirrhosis. Magnetic Resonance Elastography (MRE) is another non-invasive imaging method that can be used to stage NAFLD [15]. It measures the stiffness of soft tissues by introducing shear waves and imaging their propagation using MRI. Huwart et al. [15] showed that MRE is superior to Ultrasound Elastography (UE) and is a reproducible method that has been applied in NAFLD [14].

1.1 Diffusion-weighted imaging

1.1.1 Molecular Diffusion

Diffusion is essentially the thermal random motion of molecules in a medium at temperatures above absolute zero and it is a function of temperature, viscosity and particle size. The Einstein equation [13] describes the behaviour of unrestricted diffusion according to:

$$r_{rms} = \sqrt{2Dt} \quad (1.1)$$

Where r_{rms} is the one dimensional root-mean-squared particle displacement, t is the diffusion time and D is the diffusion coefficient (mm^2/s).

In tissues, the diffusion of water molecules is not unrestricted, but it is rather affected by the constraining presence of macromolecules and other cellular (subcellular) structures. Generally, diffusion in tissues is anisotropic, since the existent restrictions do not have spherical symmetry. The directional dependence of the diffusion coefficient can be described by a 3×3 matrix, known as diffusion tensor:

$$\overline{\overline{D}} = \begin{bmatrix} D_{xx} & D_{xy} & D_{xz} \\ D_{xy} & D_{yy} & D_{yz} \\ D_{xz} & D_{yz} & D_{zz} \end{bmatrix} \quad (1.2)$$

Matrix elements D_{ii} on the diagonal correspond to the diffusion coefficients along each axis; the non-diagonal elements D_{ij} represent the degree of correlation between random motion in two different directions i and j. The tensor formulation of diffusion is the basis for imaging techniques such as Diffusion Tensor Imaging (DTI), which is often used for fiber tracking in the brain [16].

1.1.2 Imaging

Carr and Purcell [17] observed that in the presence of a magnetic field gradient, the diffusion of water molecules causes phase dispersion of the average transverse magnetization of the sample, which causes MR signal attenuation. In DWI, image contrast is sensitized to diffusion through the introduction of strong diffusion-weighting gradients prior to the imaging acquisition module. These gradients are used to increase the sensitivity of pulse sequences to molecular motion due to diffusion. An inherent problem to DWI is that by introducing diffusion gradients, the pulse sequence also becomes more sensitive to other types of motion (e.g. bulk motion), which can cause severe image artifacts that are difficult to correct. In order to prevent this, single-shot pulse sequences, such as single-shot echo-planar imaging (ss-EPI), RARE (Rapid acquisition with relaxation enhancement), or spirals are commonly used [13].

Single-shot SE-EPI (ssSE-EPI) (fig. 1.2) is the most commonly used sequence for diffusion imaging because it is very fast and insensitive to motion. In the conventional implementation of this pulse sequence, the EPI readout follows the diffusion SE preparation module which consists of a 90° excitation pulse followed by a 180° refocusing pulse. The diffusion gradients are positioned on both sides of the 180° pulse and are usually played at the maximum amplitude that is allowed by the hardware.

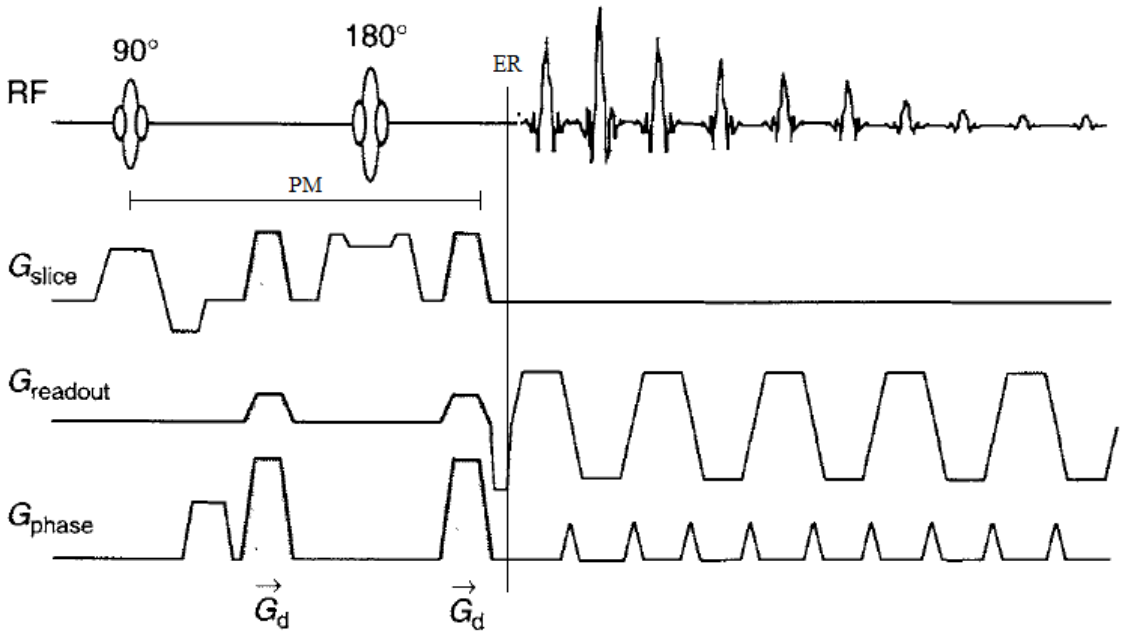

Figure 1.1 - A diffusion-weighted single-shot spin-echo EPI pulse sequence, where PM is the preparation module and ER is the EPI readout; adapted from [13].

Despite its common use, EPI has several disadvantages such as geometric distortion due to B0 inhomogeneities, low spatial resolution and limitation to 2D acquisition [13]. Parallel imaging can reduce artifacts due to B0 inhomogeneities, by reducing the echo train length

(ETL) in the EPI readout. A smaller ETL reduces the amount of time that off-resonance spins have to accumulate phase errors, thus minimizing image geometric distortions.

The fact that SE-EPI combines atypically large Eddy currents, caused by the large amplitude diffusion-weighting gradients, with an eddy current-sensitive EPI readout, also contributes to image spatial distortion, which is dependent on the direction of the applied diffusion gradient [18]. A commonly used method to overcome this problem is the one introduced by Reese et al [18], which is based on employing twice-refocused RF spin echoes with two bipolar diffusion gradient pairs to more efficiently cancel the Eddy currents (fig. 1.3).

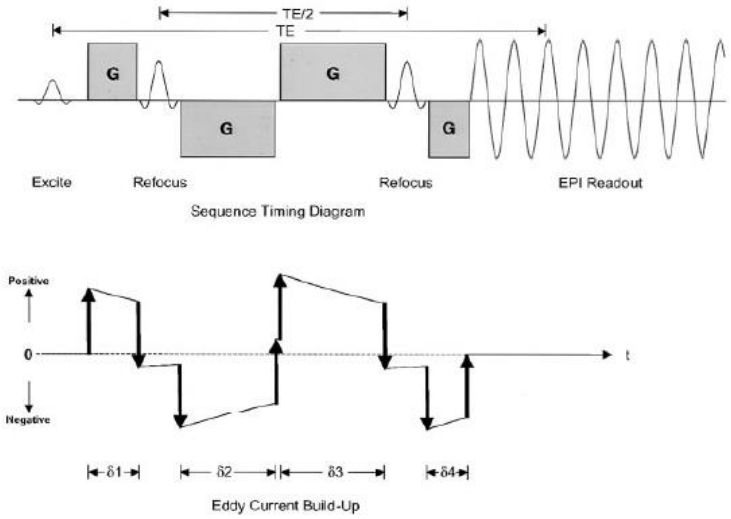

Figure 1.2 - Twice Refocused SE sequence shown as a timing diagram. This sequence allows any diffusion gradient lengths such that the rephasing and dephasing due to the diffusion gradients are equal and TE/2 is the time between the two refocusing pulses. The graph below shows the buildup and decay of eddy currents due to the gradient switching; adapted from [18].

In an ideal sequence, where the RF pulse durations and gradient ramping times are infinitely short, the timing constants in fig. 1.2 are related according to:

$$\delta_1 + \delta_2 = \delta_3 + \delta_4$$

$$\delta_2 + \delta_3 = \frac{TE}{2} \qquad (1.3)$$

$$\delta_1 + \delta_4 = \frac{TE}{2} - t_{pr}$$

where TE is the echo time, $\delta_1 + \delta_2$ and $\delta_3 + \delta_4$ are the lengths of the two bipolar field gradients, t_{pr} is the sum of the preparation time following the excitation pulse and the readout time preceding the SE. As we have four unknowns and three equations, one of the gradient lengths δ_i can be chosen. This design allows for timing flexibility which is introduced by the second

refocusing pulse. Furthermore, if the Eddy current decay time constant is known, gradient lengths can be calculated so that Eddy current build-up is nulled prior to readout.

Diffusion weighting in DWI increases with b-value, which depends not only on the amplitude and shape of the diffusion gradients but also on their duration and timing. The b-value is related to the diffusion-weighting gradient waveform $\vec{G}(t')$ by:

$$b = \gamma^2 \int_0^{TE} \left[\int_0^t G(t') \quad dt' \right]^2 dt \quad (1.4)$$

where γ is the gyromagnetic ratio and t is time

Figure 1.3 shows the explicit dependence of b on gradient parameters for commonly used diffusion-gradient waveforms in SE-EPI sequences.

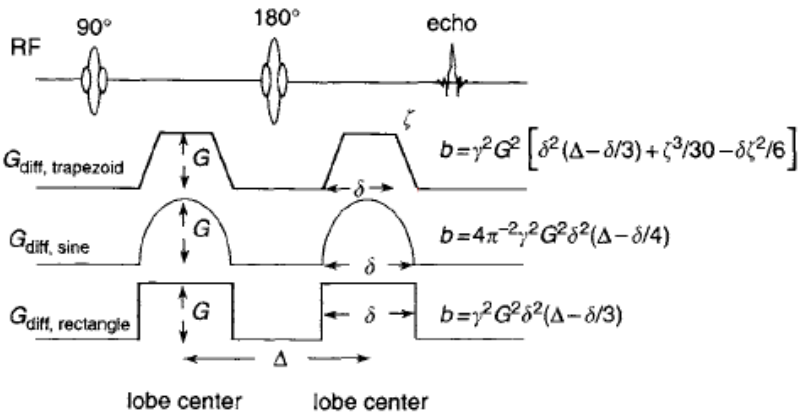

Figure 1.3 - b-values for commonly used diffusion-gradient waveforms in SE pulse sequences; adapted from [13].

In order to achieve b-values on the order of 1000 s/mm^2, the diffusion-weighting gradient lobe is typically several tens of milliseconds in length, which leads to a long TE. On the other hand, a long TE reduces the SNR and introduces T2-weighting in the diffusion-weighted image (T2 shine-through [13]). The TE can be reduced by playing-out the diffusion gradients at their maximum slew rate. However, the use of maximum gradient slew rate can cause the pulse sequence to exceed the limits for peripheral nerve stimulation and increase the problems caused by eddy-currents induced by the diffusion-weighting gradient. For this reason, the common practice to shorten TE is to use the maximum possible gradient amplitude to achieve the desired b-value.

1.1.3 Signal modelling

In the presence of a gradient, molecular diffusion attenuates the MR signal according to:

$$S = S_0 e^{-bD} \quad (1.5)$$

where S and S_0 are the voxel signal intensities with and without diffusion weighting respectively, D is the diffusion coefficient and b is the b-value.

Contrary to what happens in DTI, the approach in (1.3) does not take the directional dependence of D into account. However, the contrast of a DW image can change due to patient orientation. In order to remove this spatial dependence from the image contrast, three DW images, corresponding to diffusion gradients applied along three orthogonal directions, can be used. If S_x, S_y and S_z are signal intensities measured in each of the three images, then the following relations hold:

$$S_x = S_0 e^{-b_{xx} D_{xx}}$$

$$S_y = S_0 e^{-b_{yy} D_{yy}} \quad (1.6)$$

$$S_z = S_0 e^{-b_{zz} D_{zz}}$$

Where b_{xx}, b_{yy}, and b_{zz} are the b-values associated with each of the diffusion gradient directions. If the same b-value is used in all three directions, the geometric mean of the signals is:

$$S_{xyz} = \sqrt[3]{S_x S_y S_z} = S_0 e^{-b(D_{xx}+D_{yy}+D_{zz})/3} = S_0 e^{-bD_{trace}/3} \quad (1.7)$$

Where D_{trace} is the sum of the diagonal elements of the matrix in Eq. (1.2). The trace is rotationally invariant, i.e. it has exactly the same value independently of the rotation applied to the coordinate system, which implies that S_{xyz} is independent of the patient orientation.

In practice, signal attenuation in DWI is due to molecular diffusion and perfusion. The origin of the perfusion effect in signal attenuation lies in the movement of spins within randomly oriented capillaries, which mimics a pseudo-diffusion motion. The mathematical formalism describing both effects in signal attenuation is explained in section 2.1.

1.2 The clinical application of Intravoxel Incoherent Motion – Diffusion Weighted Imaging (IVIM-DWI) in NAFLD – Literature review

In conventional DWI, it is assumed that the signal decay has a mono-exponential behaviour as a function of b-value and that it is controlled by the value of the Apparent

Diffusion Coefficient (ADC). This coefficient is said to be apparent because it does not only measure the effect of molecular diffusion in tissues, but also the effect of the pseudo-diffusion in the capillary network within these tissues. Therefore, the signal variation that is measured from tissues with DWI as a function of b is better described by a bi-exponential model, which contains both the contributions from molecular diffusion (D) and pseudo-diffusion (D*) due to perfusion [19]. If for brain tissues, where the fraction of perfusion is low (<4%) [20], the mono-exponential model is a good approximation, that is not the case for e.g. the liver, where the fraction of perfusion in the tissue is approximately 30% [21].

Intravoxel incoherent motion (IVIM) imaging is a method to quantitatively evaluate the microscopic translational motion that occurs in each image voxel [22]. In IVIM-DWI, images are acquired at multiple b-values and it has been shown [22] that it is capable of distinguishing D from D^*. The relation between signal variation and b-values in the context of IVIM was described by Le Bihan [19] as:

$$\frac{S_b}{S_0} = (1 - fp) \cdot \exp(-bD) + fp \cdot \exp(-b(D + D^*)) \quad (1.8)$$

where S_b is the signal intensity for a given b-value, S_0 is the signal intensity for b equal to zero, fp is the fraction of perfusion, D is the pure molecular diffusion (slow component), and D^* is the pseudo-diffusion, or fast component [22].

Several studies have tried to show the clinical application of IVIM-DWI to liver imaging [4, 19, 20]. In [22] IVIM-DWI using 10 b-values was applied in the calculation of diffusion parameters in patients with cirrhosis. It was concluded that both D* and ADC are significantly reduced in cirrhotic patients when compared to healthy controls, while fp and D were similar in both groups. This appears to imply that in cirrhotic livers changes in liver architecture are of less importance when compared to changes in liver perfusion. However, the conclusions in [5] point in a slightly different direction. Here IVIM-DWI analysis was applied to an animal model of cirrhosis and results showed that in cirrhotic livers, both D* and D were decreased when compared to healthy liver. Contrary to [22], this suggests that both molecular diffusion and perfusion contribute to the changes in ADC observed in cirrhotic livers.

Patel et al. [6] studied the use of IVIM DW-MRI and DCE-MRI alone and in combination for the diagnosis of liver cirrhosis. Their study suggested that all diffusion parameters (ADC, D*, D, f) were significantly reduced in the cirrhotic group when compared to the non-cirrhotic group. Although DCE-MRI results showed that both portal venous flow and total liver flow were decreased in cirrhosis, a significant correlation between CE-MRI and IVIM-DWI parameters was not found.

Poyraz et al. [2] have studied the use of diffusion-weighted MRI on fatty liver. Their study indicated that liver fat content affected the ADC, and found a significant inverse correlation between hepatic fat fraction (HFF) measured by chemical shift GRE imaging and the

ADC on DWI. The inverse correlation between HFF and ADC could be explained by the fact that increasing fat content of liver cells and extracellular fat accumulation would lead to reduced interstitial space and consequent increased restriction to water diffusion, resulting in lower ADCs. Guiu et al. [23], used IVIM DWI to study the difference between D, D* and fp in patients with type 2 diabetes with and without liver steatosis. Results showed that while D and D* are significantly decreased in steatotic when compared to non-steatotic livers, fp shows the opposite behaviour. It is suggested that the presence of large fat droplets in the cytoplasm of hepatocytes causes the displacement of the remaining contents of the cell peripherally, which leads to the decreased mobility of water molecules in the extra-cellular environment. In addition, the decrease in D* indicates that this structural change is associated with decreased parenchymal perfusion. Finally, the increase in fp is probably due to the shorter T2 of the tissue compartment signal, when compared to that of the vascular compartment, which causes an overestimation of the signal fraction of the vascular compartment [17, 20].

1.3 Optimal b-value distribution

The importance of the choice of b-value distribution for IVIM-DWI data acquisition on parameter estimation has been stressed by several authors. In [20], Lemke et al. suggested that for an optimal estimation of the diffusion coefficient, additional higher b-values should be used, since their study only had one b-value higher than 200 s/mm^2. In [6], Patel et al. attributed the absence of differences between normal and cirrhotic livers using IVIM parameters, obtained in previous studies, to the limited number of b-values used, especially below 200 s/mm^2. Chandarana et al. [21], stated that there is no actual consensus about which b-values are optimal for liver imaging, and that their choice was completely arbitrary and based on the investigator's experience and type of protocol. Zhang et al. [24], pointed that one of the key points of the IVIM model was the selection of proper b-values in order to provide maximum precision of diffusion parameters. Finally, Lemke et al. [20] evaluated the extent to which the bi-exponential signal decay could be attributed to the vascular compartment. Their study verified that the signal decay in IVIM-DWI of the pancreas in human in-vivo experiments was strongly influenced by the vascular component (fraction of perfusion>11%). Furthermore, it was observed that there was a significant increase of the fraction of perfusion with TE whereas the same type of dependence could not be observed in D and D*. It is suggested that this dependence is artificially created by the large difference between the T2 relaxation times of blood (T2=290 ms @ 1.5T) and (pancreatic) tissue (T2=46 ms @ 1.5T). In this situation, the signal drop in the lower b-value range is larger for the short than for the long T2 species, which leads to an overestimation of the fraction of perfusion. This dependence disappears when the T2 relaxation effects are taken into account in the computation of fp, D and D*.

Although the calculation of diffusion parameters using IVIM-DWI is potentially very dependent on image acquisition parameters (e.g. TE, b-values) and T2 relaxation effects [17, 20], the truth remains that most clinical applications of IVIM-DWI rely on an empirical choice of b-values and few studies have so far tackled the problem of systematically studying the

effects of b-value distribution on IVIM parameter estimation. In the studies of Lemke et al. [25] and Zhang et al. [24], two different methods have been respectively proposed to tackle the problem of selecting the optimal b-value distribution to decrease the errors of IVIM-DWI estimations. In [25], the optimal b-value distribution is obtained through Monte Carlo Simulations. In this method, optimum b-value distribution is searched by consecutively adding new b-values to the b-value sequence, performing Monte Carlo Simulations in each iteration in order to compute the relative errors of each IVIM parameter as:

$$\sigma_f = \left(\frac{\sqrt{\frac{1}{N}\sum_{i=1}^{N}(fp_i - fp)^2}}{fp} \right) \times 100\%$$

$$\sigma_D = \left(\frac{\sqrt{\frac{1}{N}\sum_{i=1}^{N}(D_i - D)^2}}{D} \right) \times 100\% \quad (1.9)$$

$$\sigma_{D^*} = \left(\frac{\sqrt{\frac{1}{N}\sum_{i=1}^{N}({D^*}_i - D^*)^2}}{D^*} \right) \times 100\%$$

And the relative overall error is:

$$\sigma = \sigma_{fp} + \sigma_D + \sigma_{D^*} \quad (1.10)$$

where, fp_i, D_i and D_i* are the fitted results of the ith repetition and fp, D and D* the values of the selected parameter set. The values, fp, D and D* are used to calculate the individual relatives errors instead. The optimal b-value distribution is selected by choosing the one that minimizes the overall error in 1.10. The main limitation of this method is that it is not certain that the obtained b-values are optimal for any number of b-values.

In [24], the optimal b-value distribution is calculated through the minimization, in a least squares sense, of an error propagation factor. This study considered that in the process of model fitting, random noise in the DWI signal would propagate into the estimate of the model parameters. It assumes that given a set of biexponential parameters and a set of b-values, an error propagation factor for each IVIM model parameter could be predicted (mathematically explained in section 2.1.2). Furthermore, it assumes that each parameter may contribute differently to the total propagated error.

In this work, the effects of chosen b-value sequences and T2 relaxation effects on the error and bias associated with S0, fp, D, and D*, using the method presented in [24], will be systematically studied in both simulation studies and in-vivo experiments.

2. Materials and Methods[1]

2.1 Optimization of b-value distribution through the minimization of an error propagation factor

Considering equation (1.8), since D^* is approximately two orders of magnitude greater than D, its influence can be neglected for b-values higher than 200 sec/mm^2 [5] and D can be straightforwardly computed by a linear fit to the following expression:

$$ln(S_b) = -Db + ln(S_0) \quad (2.1)$$

Once D is known, fp and D* can be computed by performing a non-linear fit of the data to (1.8), in a least-squares sense, using the Levenberg-Marquardt method [24] and the cost function R'(fp, D, D*):

$$R'(fp, D, D^*) = \sum_i \left(S_i'(b_i, D, D^*, fp) - S'_{i,Data}\right)^2 \quad (2.2)$$

Where S'_i and $S'_{i,Data}$ are the normalized signal intensities, computed as in (1.8) and measured experimentally (for $b=b_i$) respectively.

The calculation of D, D* and fp in two-steps greatly simplifies the computations, in particular because the number of non-linear parameters to be calculated from (1.8) reduces from three to two.

In [24], it is noted that given a set of DWI measurements at multiple b-values b_i, parameters, fp, D*, D, can be determined, in a least-squares sense by minimizing the sum of squared residues between the data and the model fit $R(S_0, fp, D, D^*)$:

$$R(S_0, fp, D, D^*) = \sum_{i=1}^{N_b} [S(b_i; S_0, fp, D, D^*) - S_{b_i}]^2 \quad (2.3)$$

where N_b is the total number of b-values and S_{bi} is the signal measured at b_i. In order to minimize (2.3), partial derivatives with respect to S_0, fp, D, and D^* have to be nulled:

$$\frac{\partial R}{\partial x(m)} = \sum_{i=1}^{N_b} \left\{ 2 \cdot \left[S(b_i, x) - S_{b_i}\right] \cdot \frac{\partial S(b_i, x)}{\partial x(m)} \right\} = 0, \quad m = 1,2,3,4 \quad (2.4)$$

[1] The algorithms that are presented in this chapter were implemented in Matlab (The Mathworks Inc., Natick, MA).

where x(m) (m = 1, 2, 3, 4) represent S_0, fp, D, and D^*, respectively.

After mathematical manipulations (see Appendix A), an error propagation factor ξ can be defined as the ratio of the relative error in a model parameter to the relative input noise δ/S_0:

$$\xi(n) = \frac{\delta x(n)/x(n)}{\delta/S_0} =$$

$$= \frac{S_0}{x(n)} \sqrt{\sum_{m=1}^{4}\sum_{p=1}^{4}\left[A^{-1}(n,m)\cdot A^{-1}(n,p)\cdot \sum_{i=1}^{N_b}\left(\frac{\partial S(b_i,x)}{\partial x(m)}\cdot\frac{\partial S(b_i,x)}{\partial x(p)}\right)\right]} \quad (2.5)$$

Where δ is the noise standard deviation, x(n) represent S_0, fp, D, and D^* and δx(n) is the column vector of estimation errors for each parameter and n runs over the number of parameters, four in this case. The elements of A^{-1} and the partial derivatives $\partial S/\partial x$ are defined as in Appendix A.

In order to calculate the total error ξ_{total} that is propagated into IVIM-DWI parameters, the errors of D, D* and fp are summed:

$$\xi_{total} = W_{fp}\xi_{fp} + W_{D^*}\xi_{D^*} + W_D\xi_D \quad (2.6)$$

Where W_{fp}, W_{D^*} and W_D are the weights associated with the error propagated into fp, D* and D respectively. The calculation of the optimum b-value distribution to estimate a given set of parameters D, D* and fp is performed by means of minimizing (2.5) with respect to b_i using the Levenberg-Marquardt method.

In practice, the IVIM-DWI signal consists of the contribution of tissues with different native D, D* and fp values. Therefore, a natural extension of (2.6) is to consider the contribution of various tissues to the total error - $\bar{\xi}_{total}$:

$$\bar{\xi}_{total} = \int_{D^{min}}^{D^{max}}\int_{D^{*min}}^{D^{*max}}\int_{f^{min}}^{f^{max}} (W_{fp}\,\xi_{fp} + W_{D^*}\xi_{D^*} + W_D\xi_D)dfpdD^*dD \quad (2.7)$$

where X^{max} and X^{min} are the expected range values of each parameter.

2.2 Simulation studies

The influence of b-value sequence and T2 relaxation effects on IVIM-DWI estimations was investigated in simulation studies that were divided in two categories. First, the dependence of the propagated error on parameters such as the number of b-values used to sample the signal (N_b), echo time (TE), spin-spin relaxation time (T_2) fraction of perfusion (fp), perfusion related diffusion (D*) and perfusion rate (PR= fp × D*) was investigated. In a second

phase, the performance of each of the b-value distributions in estimating IVIM-DWI parameters was tested against the presence of noise through Monte Carlo simulations.

In all simulations, the Levenberg-Marquardt [24] minimization algorithm was used to minimize the total propagated error (detailed in section 2.1.2) into IVIM-DWI parameters. The minimization would stop if the number of iterations exceeded 800 or if the variation of the cost function from iteration to iteration would be smaller than $1e^{-6}$. In order to avoid local minima of the cost function, the Levenberg-Marquardt algorithm was always applied to a set of twelve or thirteen different starting b-value sequences, finding then the distribution with the minimum overall propagated error, considering this the optimal b value distribution.

In the first phase of the study, the dependence of the propagated error on N_b, TE, T_2, fp, D* and PR was investigated in three steps:

1) The influence of D*, fp and N_b on the propagated error of IVIM-DWI estimations was investigated. For that, the optimal b-value sequence with equal weights was used to calculate the total and partial errors propagated to D, D* and fp. The number of b-values N_b, fp and D* were varied according to N_b=5, 8, 10 and 16, fp=0.1, 0.2, 0.3 and 0.4 and D*=0.01, 0.03, 0.08, 0.10 and 0.15. Further simulation parameters were T2=34 ms [22], D=0.00123 mm^2/s [22], S0 =100, and considering no transverse relaxation effects.
2) The influence of b-value distribution on the propagated error of IVIM-DWI estimations was investigated. The same simulation parameters of the previous step were used, using optimum b-value sequence with equal weights and conventional sequence and comparing results obtained with each.
3) The influence of PR variation on the propagated error of IVIM-DWI estimations was investigated. For that, the same simulation parameters were used and PR was varied in a fixed interval in two different ways. In the first situation, PR was varied by changing D*, while keeping fp fixed (=0.3), whereas in the second situation the reciprocal was considered (D*=0.08 mm^2/s). Parameter PR was varied according to PR=0.003, 0.006, 0.009, 0.012, 0.015, 0.018, 0.021, 0.024, 0.027, 0.030, 0.033, 0.036, 0.039, 0.042 and 0.045.

In a second phase, the performance of each of the b-value distributions in estimating IVIM-DWI parameters was tested against the presence of noise through the performance of Monte Carlo simulations (detailed in section 1.3), using three types of b-value combinations, derived from the first set of simulations:

- *Conventional sequence*: the b-values are chosen as used in conventional clinical applications (e.g. 0 5 15 30 40 80 100 200 400 800 s/mm^2);
- *Optimum b-value sequence with equal weights*: the b-values are obtained by the minimization of 2.1 with respect to b and considering $W_f=W_{D*}=W_D=0.25$;

- *Optimum b-value sequence with different weights*: the b-values are obtained as in *Optimum b-value sequence with equal weights*, but considering that $W_f \neq W_{D^*} \neq W_D$.

Here, the propagated error was calculated not for one specific D* but for a range of D* values in the interval ranging from 0.01 to 0.15 using 2.7. The weights W_D, W_{D^*} and W_f were extracted from step three of the first phase of the study by fitting the lowest (possible) order polynomial to the data. Bias and Error presented in all results were calculated as explained in section 1.3. This phase was performed in two steps:

1) The influence of b-value distribution, noise and T2 relaxation effects on Bias and Error of IVIM-DWI estimations was investigated. For that, the three types of b-value sequences were used to calculate the Error and Bias of D, D* and fp. The number of b-values N_b and fp were 10 and 0.3, respectively. Further simulation parameters were T2=34 ms, D=0.00123 mm^2/s (liver parameters) measured at 3T [22], S0 =100. Firstly, in order to study noise influence, SNR was varied according to SNR=200, 100, 50, 40, 30 and 20 and relaxation effects were not included. Secondly, to study the influence of T2 relaxation effects, TE was varied according to TE=50, 60, 70, 80, 90 and 100ms and SNR was kept constant at 50.
2) The influence of the number of b-values on Bias and Error of IVIM-DWI estimations was investigated. For that, N_b=8, 10 and 16 were used to calculate the Error and Bias of D, D* and fp. Optimal b-value sequence with different weights and considering fp=0.3 were used. Further simulation parameters were the same as before and relaxation effects were not included.

2.3 In-vivo studies

The influence of TE and b-value sequence on IVIM-DWI estimations was investigated in in-vivo studies that were divided in two phases. First, the dependence of IVIM-DWI estimations on the number of b-values used to sample the signal (N_b) was investigated in data that had been previously acquired in the framework of a running project. The clinical population consisted of 34 diabetes type II patients (21 females and 13 males with mean age 60±8) and 40 controls (25 females and 15 males with mean age 49±7) and all gave written informed consent. The patient group consisted of men and women with type II diabetes, diagnosed at least 1 year prior, age 40-74 years. The control group was age matched to the patient group and without a history of neuropsychiatric, renal, liver, heart, ocular or any other severe non-age related disease, not related to diabetes. A sub-group of 10 patients having Steatosis was created.

Magnetic resonance liver imaging was performed on a whole body 3T imaging system (Magnetom Trio Tim, Siemens Medical Solutions, Erlangen, Germany) using a 4-channel or a 16-channel body coil. Respiratory triggered IVIM imaging was acquired using conventional SE-EPI with acquisition parameters: FOV=400×400 mm, 3.12×3.12

mm in-plane resolution, 1 slice 10 mm thick, TR/TE=3800/67 ms, parallel imaging factor 2, 3 or 5 averages using the 4- or 16-channel coil respectively, 16 b-values (0, 5, 10, 15, 20, 25, 30, 35, 40, 50, 70, 90, 100, 200, 400, 800). IVIM-DWI estimations using these data were recomputed with 8 (0, 20, 40, 80, 100, 200, 400, 800) and 10 (0, 5, 15, 30, 40, 80, 100, 200, 400, 800) b-values, and compared with the original estimations that were obtained with 16 b-values.

In a second phase, the performance of each of the b-value distributions, conventional sequence, optimum b-value sequence with equal weights and optimum b-value sequence with different weights, as well as the influence of T2 relaxation effects in estimating IVIM-DWI parameters was tested in healthy volunteers. Eight healthy volunteers (4 females and 4 males, mean age 22±1) were enrolled and gave written informed consent. This volunteers were separated in two groups, one to study the influence of T2 relaxation effects with 2 volunteers (2 females, with 22 and 24 years old), and the other one to study the performance of each b-value distribution (2 females, 4 males, mean age of 22±1).

On the first group, magnetic resonance liver imaging was performed on a whole body 3T imaging system (Magnetom Trio Tim, Siemens Medical Solutions, Erlangen, Germany) using a 16-channel body coil. Respiratory triggered IVIM imaging was acquired using conventional SE-EPI with acquisition parameters: FOV= 300×300 mm, 3.12×3.12 mm in-plane resolution, 1 slice 10 mm thick, TR/TE=3800/67(80) ms, parallel imaging factor 2, allowing the study of the influence of T2 relaxation effects by varying TE (67 and 80ms).

On the second group, respiratory triggered IVIM imaging was acquired using conventional SE-EPI with acquisition parameters: FOV=390×390 mm (male patients) and 300×300 mm (female patients), 3.12×3.12 mm in-plane resolution, 1 slice 10 mm thick, TR/TE=3800/67 ms, parallel imaging factor 2, 3 , 10 b-values: conventional sequence (0, 5, 15, 30, 40, 80, 100, 200, 400, 800), optimum b-value equal weighted sequence (0, 0, 15, 65, 112, 133, 208, 243, 340, 800) and optimum b-value different weighted sequence (0, 0, 9, 13, 38, 70, 90, 153, 220, 800).

3. Results

3.1 Simulation studies

3.1.1 Influence of D, fp and number of b-values on the relative and total propagated error of IVIM-DWI estimations*

The influence of D*, fp and N_b on the relative and total propagated error of IVIM-DWI estimation was studied. In figs 3.1 and 3.2, it is possible to notice the differences in the total error, while varying PR by fixing D* or fp, as well as the differences using various N_b values. Figure 3.3 shows the influence of varying PR with fixed D* on the relative error of each IVIM-DWI estimated parameter.

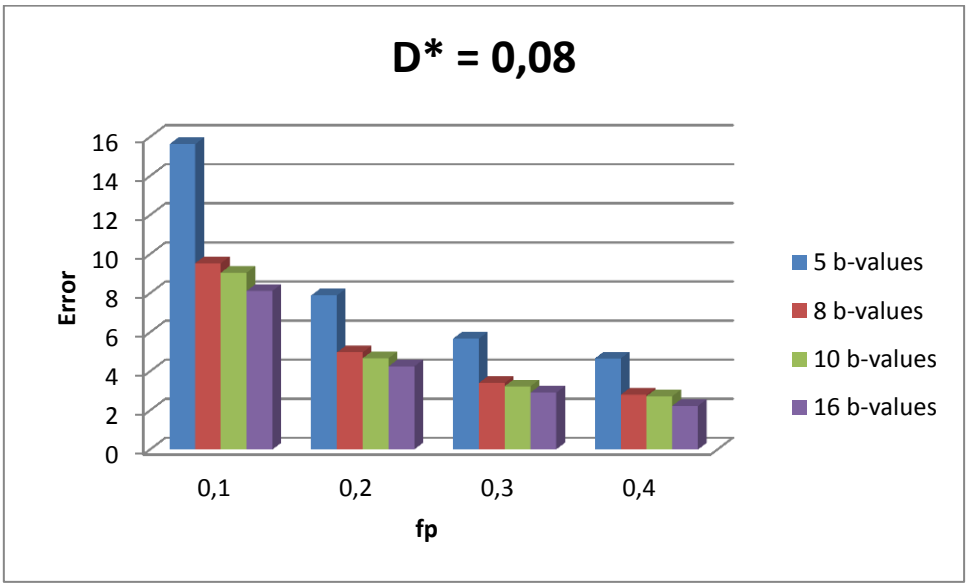

Figure 3.1 – Influence of the number of b-values and fraction of perfusion (fp) in the total error for D*=0,08mm^2/s.

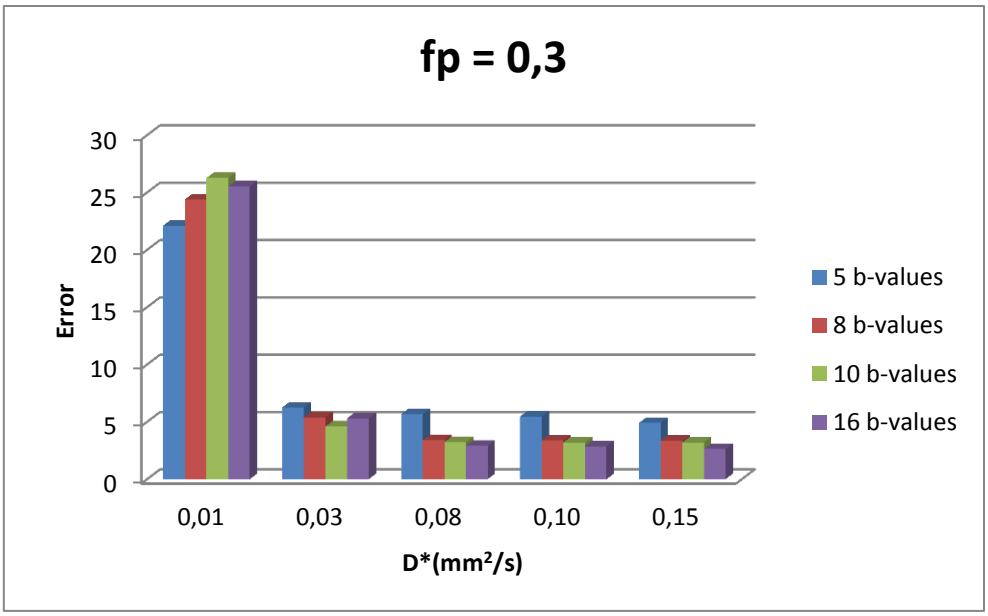

Figure 3.2 - Influence of number of b-values and pseudo diffusion (D*) in total error for fp=0,3.

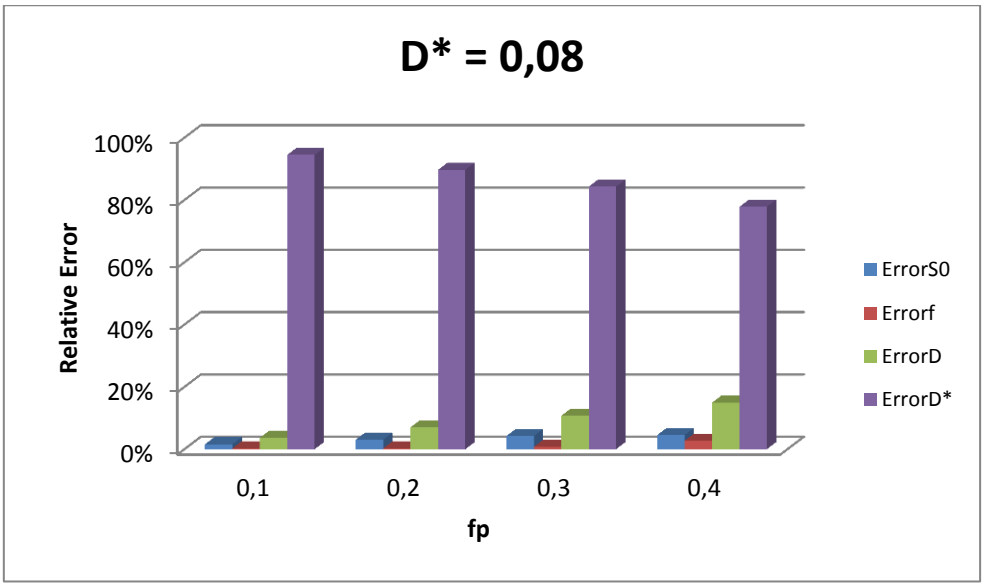

Figure 3.3 - Influence of fraction of perfusion (fp) in the relative propagated parameter error for D*=0,08 mm^2/s, considering 10 b-values.

Results show that the total error that is propagated into D, D* and fp strongly depends on the way by which the perfusion rate is varied and less so on N_b. Figures 3.1 and 3.2 show that increasing the perfusion rate (PR) by increasing fp while keeping D* fixed at the value that is currently assumed for healthy liver parenchyma [26], the error tends to decrease with both fp and N_b. On the other hand, if PR is increased by keeping fp fixed at the value that is currently assumed for healthy liver parenchyma [26], and by increasing D*, then the error still tends to decrease with the increase in PR (i.e. increase in D*). However, the error variation

with N_b depends on the value of D*. If for larger values of D*(>0.08), the error decreases with N_b, that is not so for smaller D* values. It is worth mentioning that beyond N_b=10, the error decreases only slightly. Finally, in fig. 3.3 it can be seen that D* is the parameter that most contributes to the total error, contrary to what has been assumed, and that this behaviour is independent of fp and D* (results shown in Appendix B.1).

3.1.2 Comparison between conventional b-value distribution and optimal b-value distribution with equal weights

In these simulations, the influence of the type of b-value distribution on the error propagated to IVIM-DWI parameters was studied. Figs 3.4 and 3.5 show the variation of the total error as a function of PR by respectively fixing D* or fp, for both conventional b-value distribution and optimal b-value distribution with equal weights.

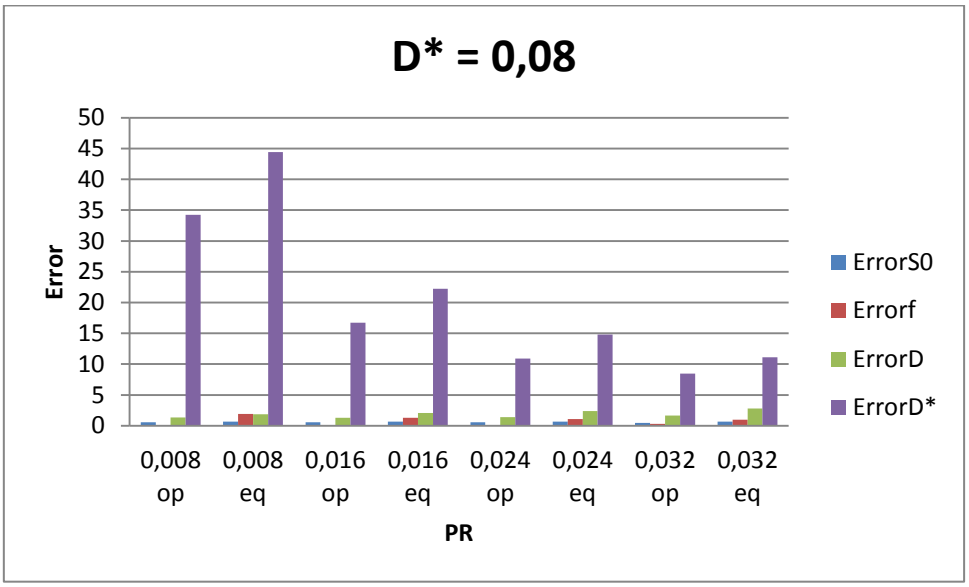

Figure 3.4 – Influence of fp in total error for conventional distribution (*eq*) and optimum b-value distribution equal weighted (*op*), considering 10 b-values in both.

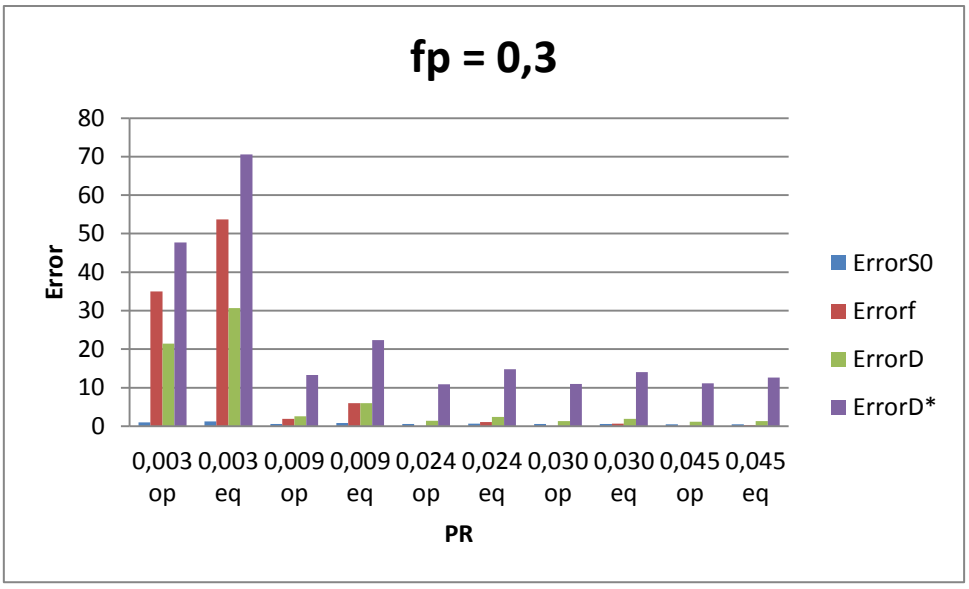

Figure 3.5 – Influence of D* in total error for conventional distribution (*eq*) and optimum b-value distribution equal weighted (*op*), considering 10 b-values in both.

Results show that the error variation of IVIM parameters as a function of PR for the conventional sequence ("eq") has a similar behaviour to that of the optimum b-value sequence with equal weights ("op"). However, even though they have a similar behaviour, the total error that is propagated to IVIM parameters strongly depends on the type of b-value sequence that is used to sample the signal, being smaller for the optimum b-value sequence with equal weights than for the conventional sequence. This behaviour is independent of the manner in which PR is varied, either changing fp or D* However, it is possible to notice that for lower values of D* (fig. 3.5) not only the error of D* is high, but also those of D and fp while the same does not hold for low values of fp (while keeping D* constant, see fig. 3.4). This suggests that error propagated to each of the IVIM-DWI parameters depends on how PR is varied. Finally, for both b-value sequences, D* is responsible for the largest fraction of the total error (>70%), independently of the value of fp and D*.

3.1.3 Comparison between D and fp variation for the same PR using the optimal b-value sequence with equal weights*

Here, the influence of PR variation on the relative error of each IVIM-DWI parameter was studied. Similary to previous simulations, PR was varied in two ways: varying fp while keeping D* fixed or vice-versa. In fig. 3.6, it is possible to notice the differences in the relative error, while increasing PR by fixing D* or fp and increasing fp or D* respectively, while keeping the same values of PR in both situations.

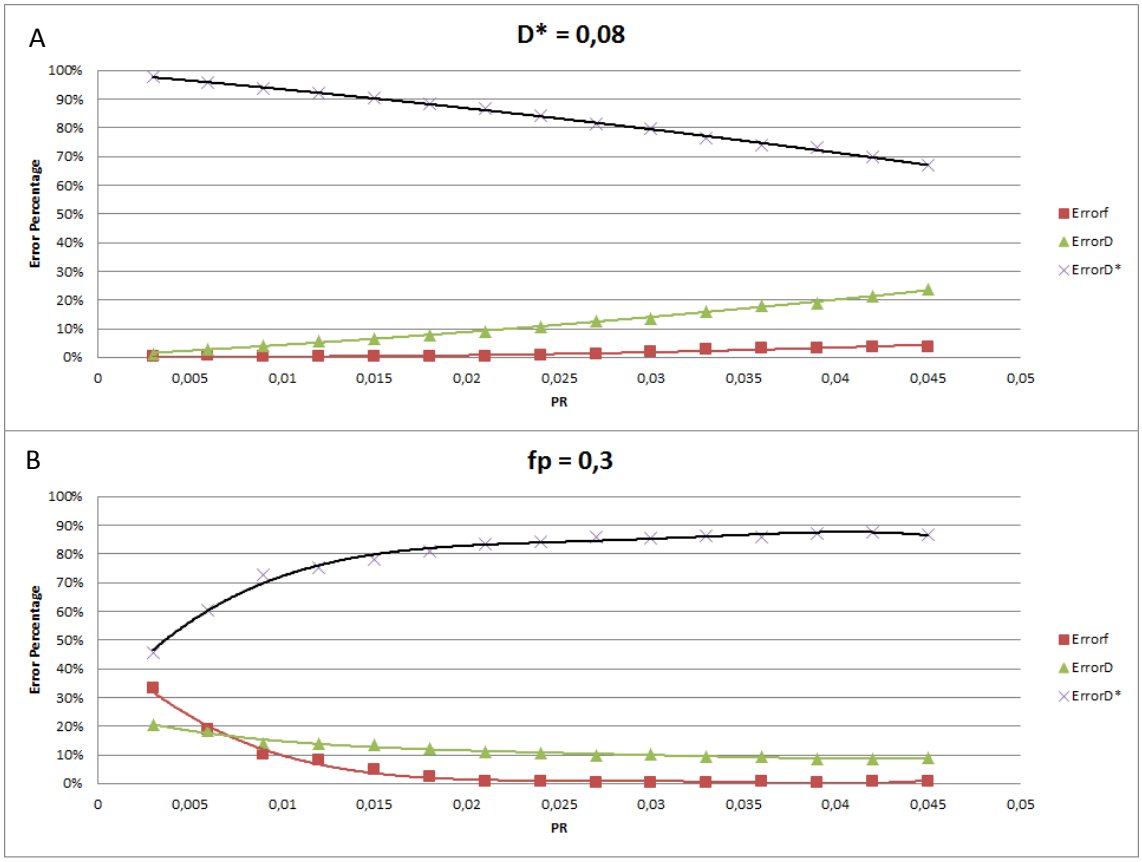

Figure 3.6 – Variation of the relative error of IVIM parameters as a function of PR : A) Constant D*and B) Constant fp, considering 10 b-values in both.

Results show that the relative errors of D, D* and fp strongly depend on the way by which PR is varied. Fig 3.6 A) shows that for increasing values of PR, by increasing fp while keeping D* fixed at the value that is currently assumed for healthy liver parenchyma [26], the relative error of D* tends to decrease, the relative error of D tends to increase and the relative error of fp remains approximately the same. On the other hand, if PR is increased by keeping fp fixed, and by increasing D*, the relative error of D* tends to increase while both relative errors of D and fp tend to decrease. However it is important to note that the D* relative error is almost always larger than 50%, thus consistently giving the largest contribution to the total error. This suggests that the error contributions from different IVIM parameters to the total error are considerably different, contrary to what has been assumed.

3.1.4 Evaluation of the number of b-values used in the optimal different weighted b-value sequence.

Results of the error and bias associated with IVIM-DWI parameters in the presence of noise are presented for the case where the sequence of b-values was optimized to minimize the errors propagated to IVIM parameters, but considering different weights for D, D* and fp.

Figs 3.7 and 3.8 respectively show the error and bias, of each IVIM-DWI parameter as a function of SNR, for different numbers of b-values and varying SNR.

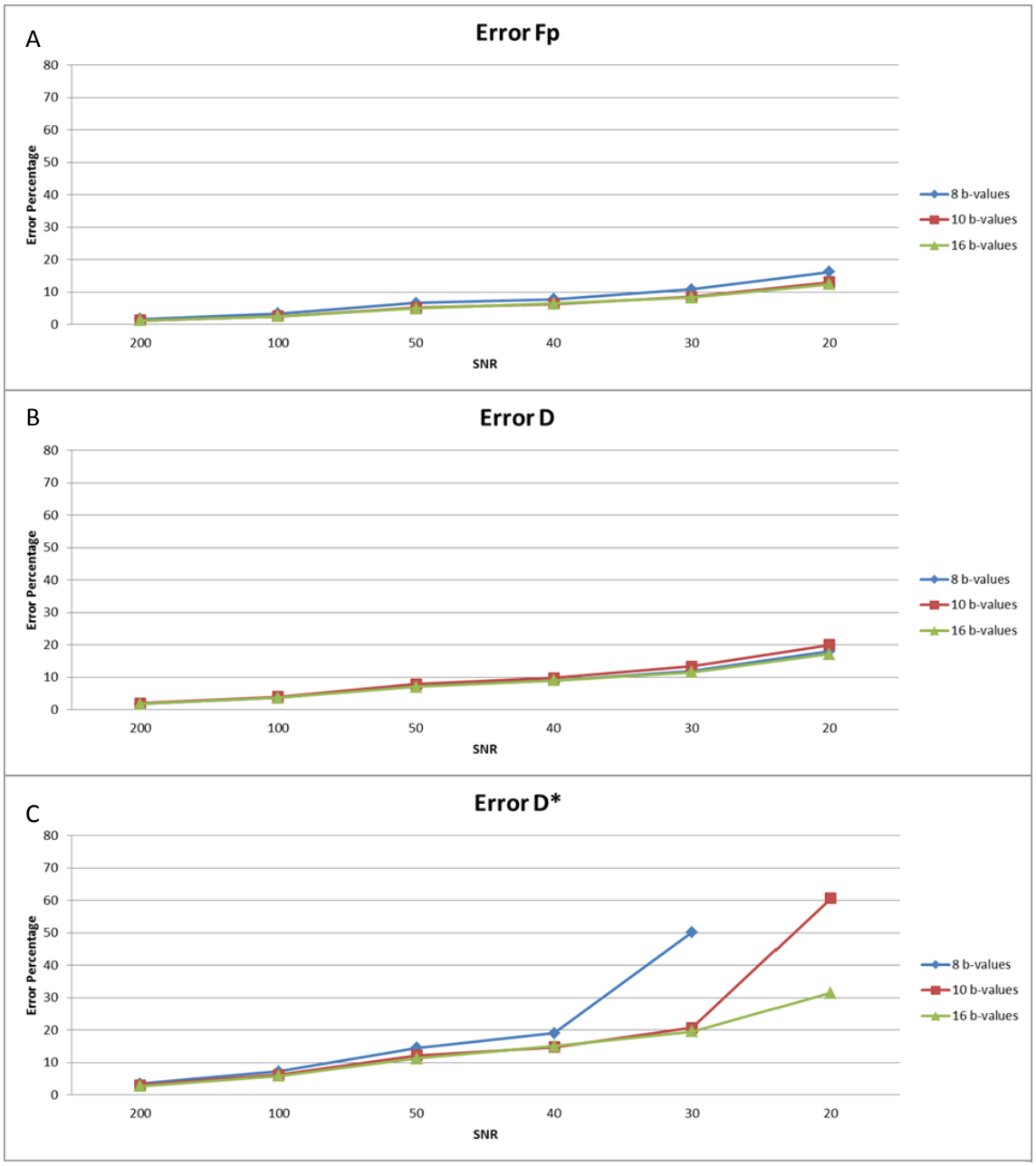

Figure 3.7 - Error percentage for: A) fp, B) D, C) D* ; with 8 (blue), 10 (red) and 16 (green) b-values, for optimum different weighted b-value sequence, fp=0.3 (note: the points not visible in the plot are considered outliers).

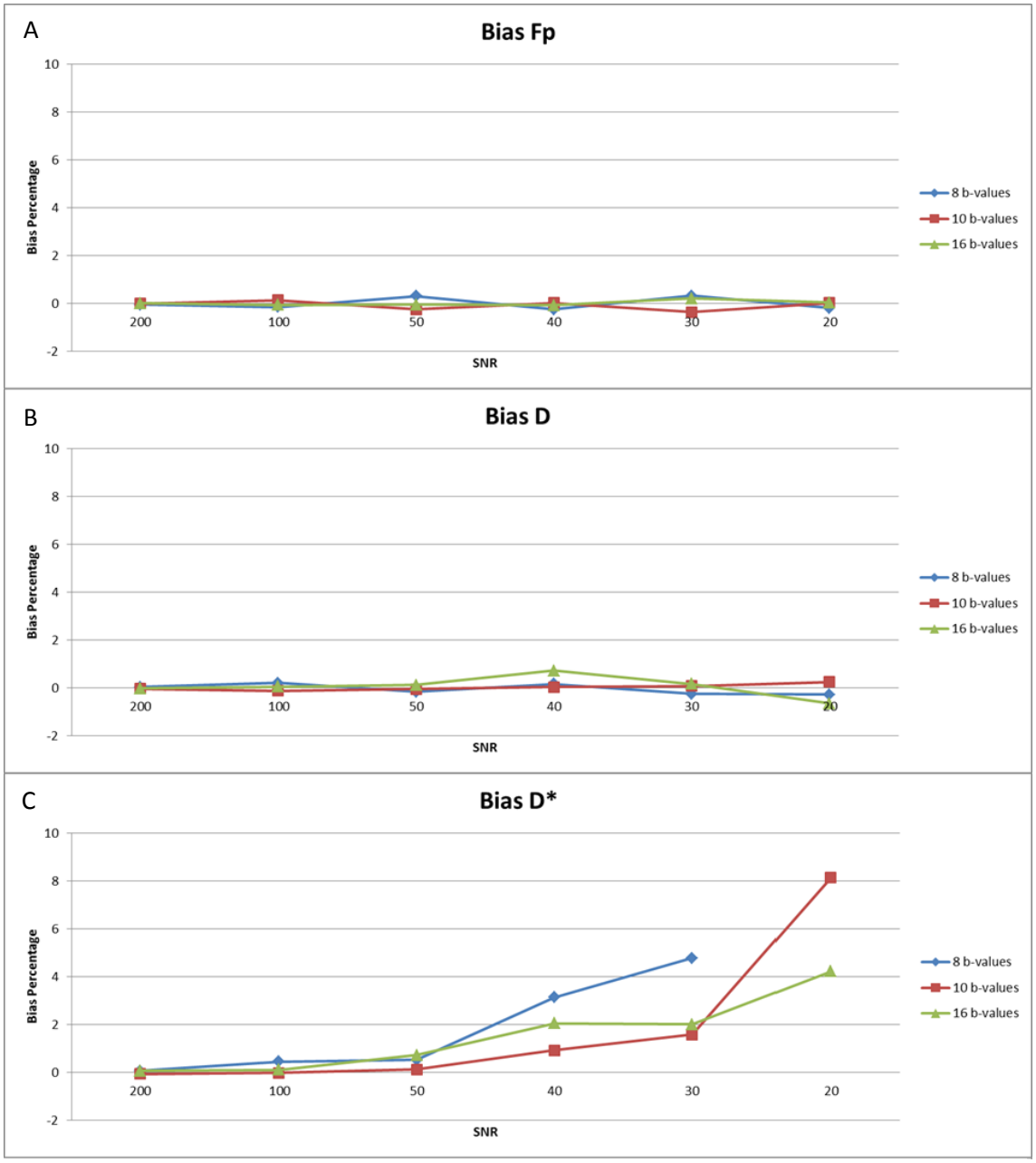

Figure 3.8 – Estimation bias for: A) fp, B) D, C) D*; with 8 (blue), 10 (red) and 16 (green) b-values, for optimum different weighted b-value sequence, fp=0.3 (note: the points not visible in the plot are considered outliers).

Results show (fig. 3.7) that independently of the SNR, the errors of D, D* and fp decrease with the number of b-values in the b-value sequence. However the same thing did not happen with respect to bias (fig. 3.8). Here, if with respect to fp and D, the number of b-values did not have a significant influence on parameter bias, the same did not hold for D*. The bias for D* is in general lower for 10 b-values except for SNR smaller than 30, where the lowest bias was obtained with 16 b-values.

3.1.5 Evaluation of the conventional distribution, optimum b-value equal-weighted distribution and optimum b-value different-weighted distribution for 10 b-values.

Simulations were carried-out in order to investigate the performance of conventional, optimal equal-weighted and optimal different-weighted b-value sequences in estimating IVIM parameters in the presence of noise. Figures 3.9 and 3.10 respectively show the variation of bias and error of fp, D and D* as a function of SNR.

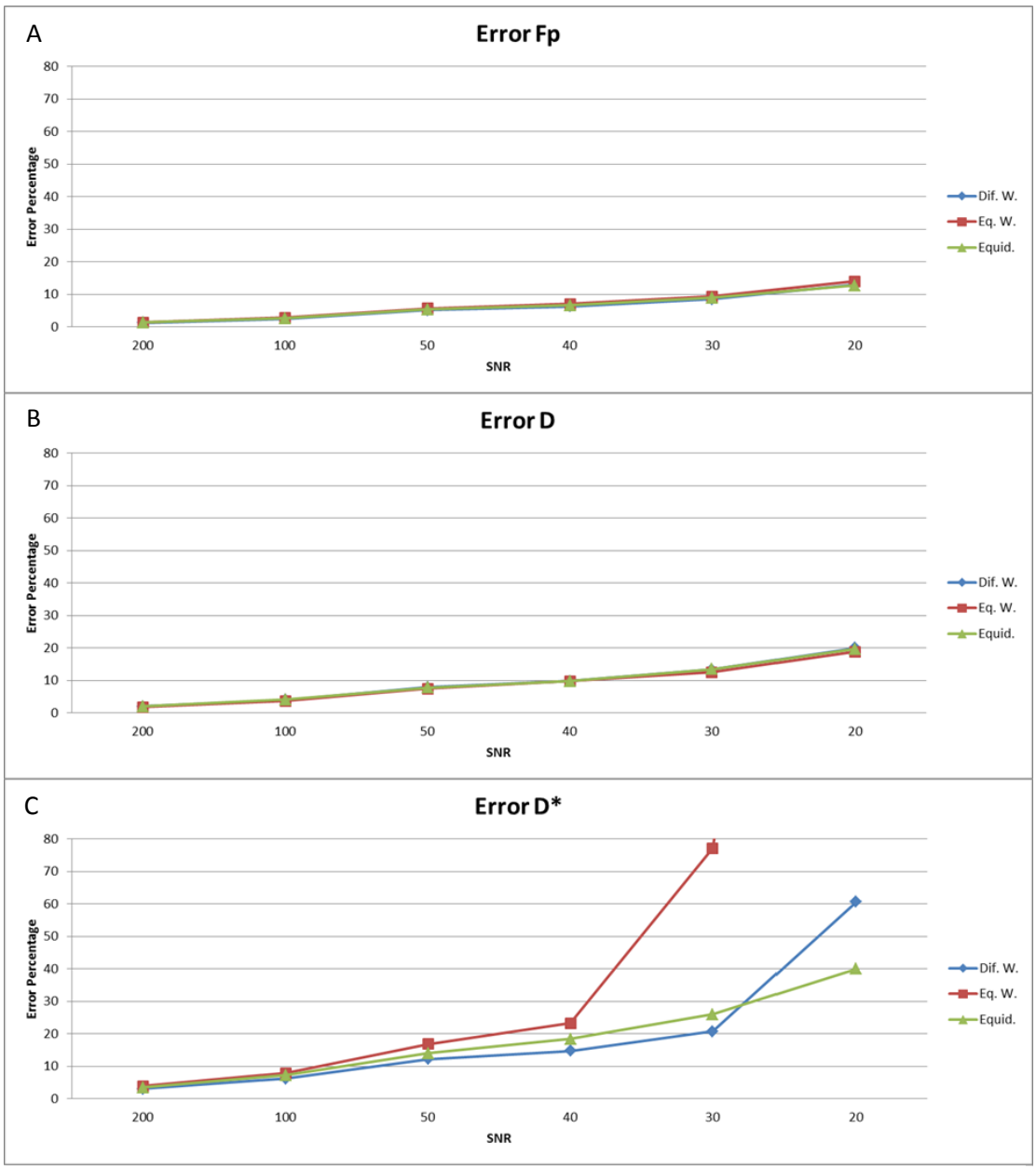

Figure 3.9 - Error for: A) fp, B) D, C) D*, with optimum different-weighted (blue), optimum equal-weighted (red) and conventional (green) b-value sequences, considering 10 b-values and fp=0.3.

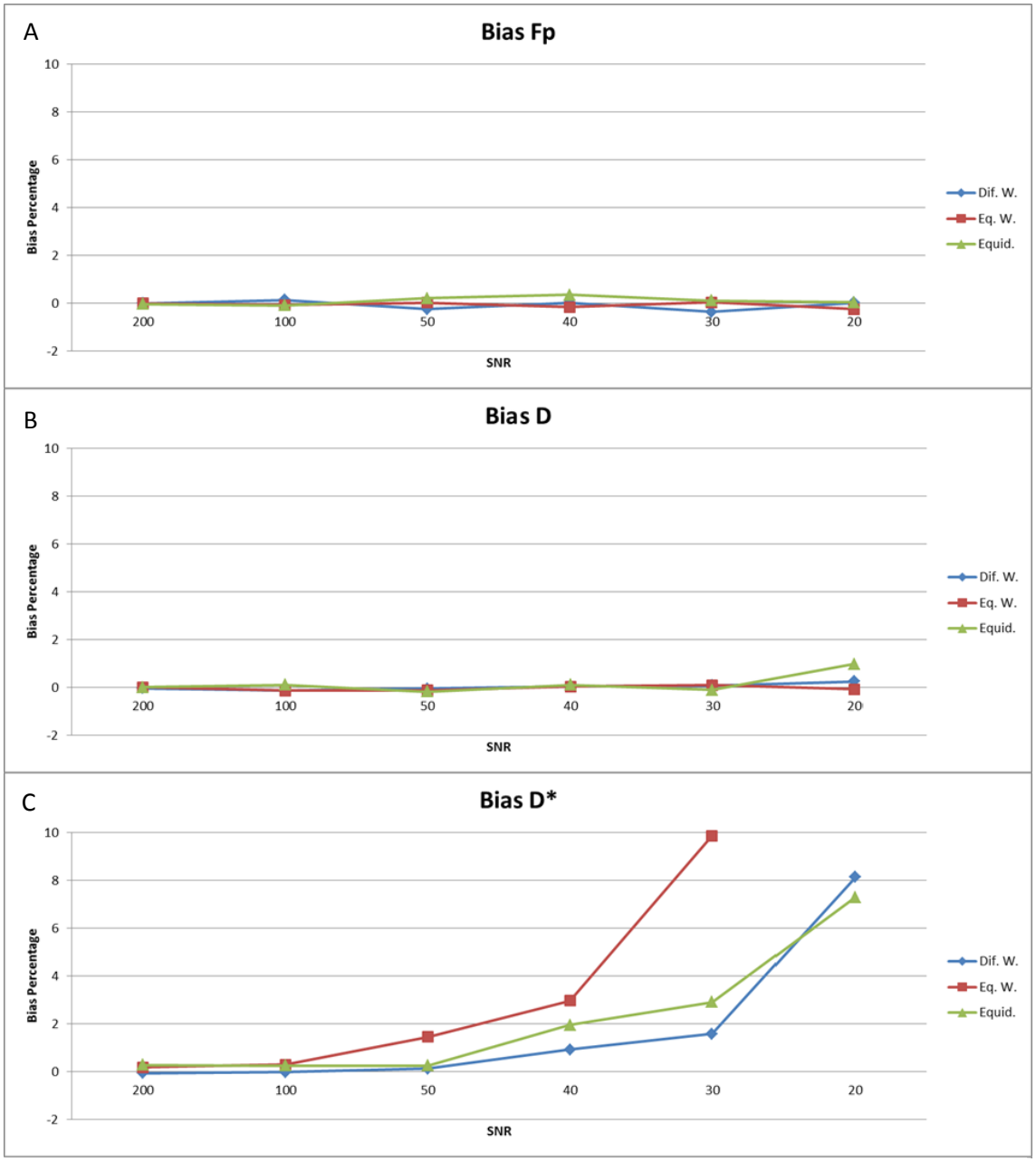

Figure 3.10 – Estimation bias for: A) fp, B) D, C) D*, with optimum different-weighted (blue), optimum equal-weighted (red) and conventional (green) b-value sequences, considering 10 b-values and fp=0.3.

Results showed that independently of the number of b-values (results not shown), the estimation error and bias for fp and D are almost equal for all sequences. However, in terms of D* this is not the case, as it can be observed from figs 3.9 and 3.10. For D*, the error and bias are generally lower for optimum b-value sequence with different weights except for SNR<30. However, in clinical practice an SNR smaller than 30 is not desirable since the estimation

significantly increases beyond this point. Therefore, in the lowest error and bias are obtained with the optimum different-weighted b-value sequence.

In the next set of simulations, the effect of T2 relaxation on IVIM-DWI parameter estimation was investigated. Figures 3.11 and 3.12 respectively show the error and bias of fp, D and D* as a function of TE for conventional, optimal equal-weighted and optimal different-weighted b-value sequences.

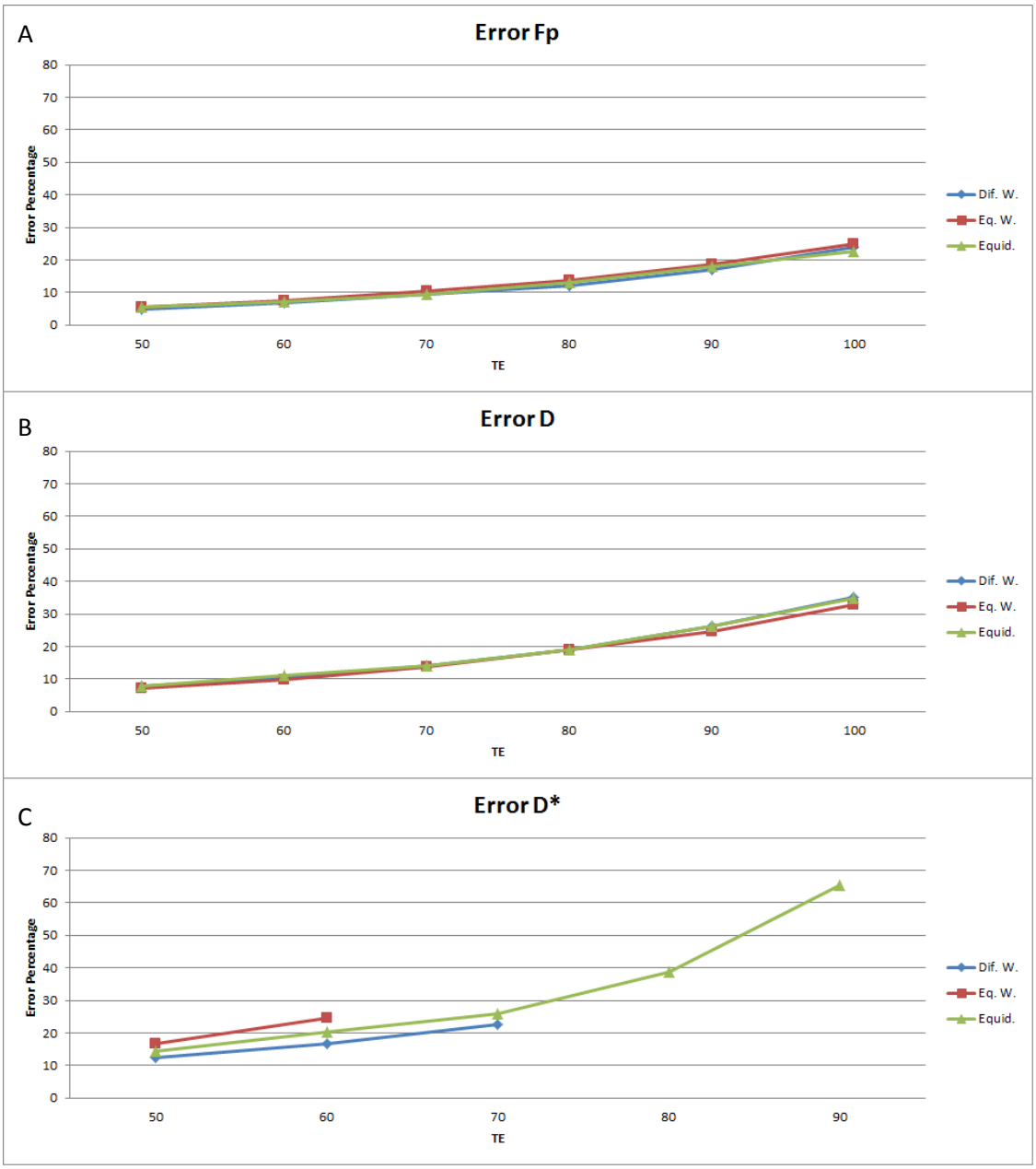

Figure 3.11 – Estimation error for: A) fp, B) D, C) D*, with optimum different-weighted (blue), optimum equal-weighted (red) and conventional (green) b-value sequences, considering 10 b-values and fp=0.3.

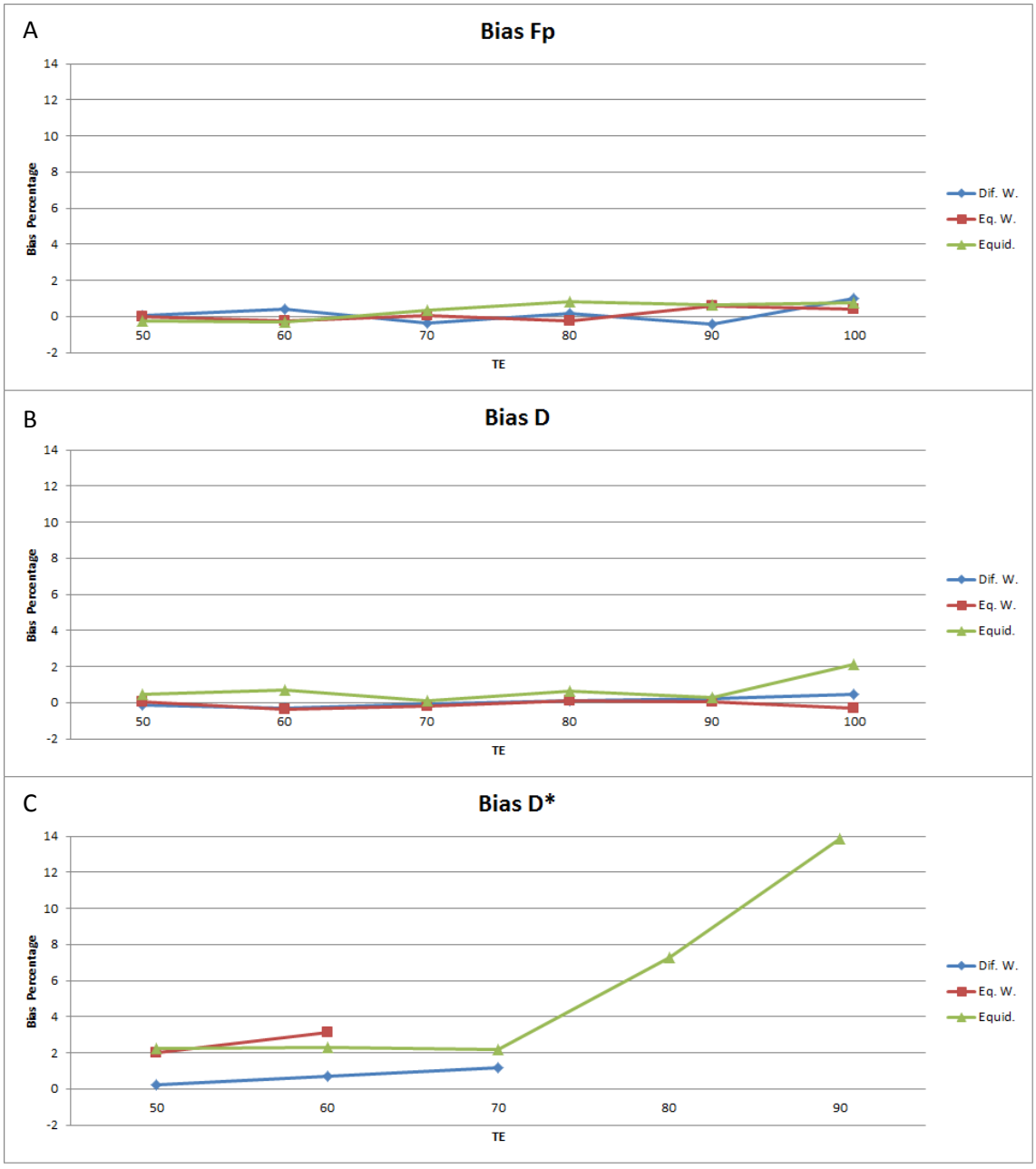

Figure 3.12 – Estimation bias for : A) fp, B) D, C) D* with optimum different-weighted (blue), optimum equal-weighted (red) and conventional (green) b-value sequences, for 10 b-values, fp=0.3 and SNR=50.

Similarly to previous results, simulations showed that independently of the number of b-values (results not shown), the estimation error and bias for fp and D are almost equal for all b-value sequences. However, in terms of D* this is not the case, as it can be observed from figs 3.11 and 3.12. The estimation error and bias of D* are generally lower for optimum b-value

sequence with different weights for TE smaller than 70. However, when SNR becomes very low due to T2 relaxation effects, i.e. for TE>70ms, the conventional distribution is actually better since it yields smaller bias and error.

3.2 In Vivo Studies

3.2.1 Evaluation of the number of b-values that is used with the conventional b-value sequence in IVIM-DWI liver studies

IVIM-DWI liver data from the clinical population that was described in "Materials and Methods" was retrospectively analysed and parameters were estimated considering b-value sequences with varying N_b values. The goal was to investigate whether the statistical significance of differences in parameters of patients and controls were independent of N_b. Figure 3.13 shows a typical example of the original IVIM-DWI data (16 data points corresponding to the total number of b-values that were considered in the acquisition) and corresponding data fit.

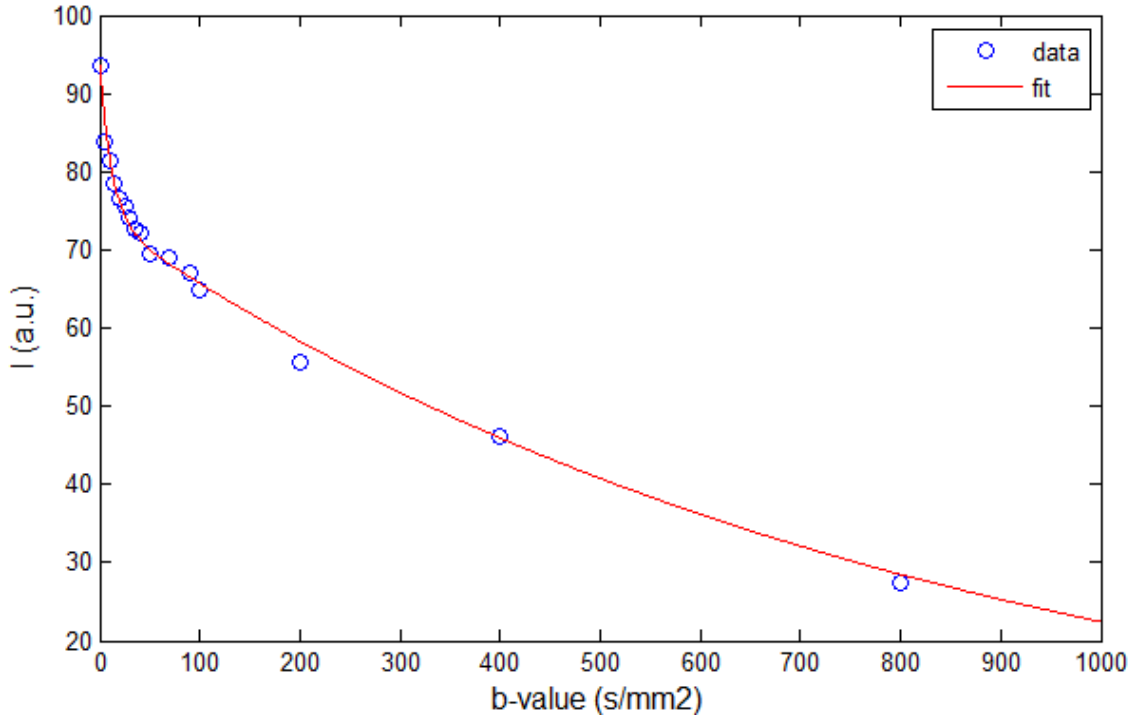

Figure 3.13 – Example of the acquired plot for a 16 b-value conventional sequence, for a Control subject.

Table 3.1 shows the mean estimation (and associated standard deviation) of D, D* and fp for patients and controls, in three different situations: 1) Considering all points in the data fit (*16 b-values*); 2) Selecting 10 out of 16 b-values (*10 b-values*); 3) Selecting 8 out of 16 b-values (*8 b-values*).

Table 3.1 - Influence of the number of b-values in in-vivo IVIM-DWI parameter estimation.

		Fp		D(*10^{-3}mm^2/s)		D*(*10^{-3}mm^2/s)	
		Mean	**StdDev**	**Mean**	**StdDev**	**Mean**	**StdDev**
Patients	**8 b-values**	0,28	0,10	1,13	0,29	45,60	23,79
	10 b-values	0,27	0,10	1,13	0,29	71,00	40,10
	16 b-values	0,26	0,09	1,13	0,29	62,23	24,85
Controls	**8 b-values**	0,30	0,12	1,15	0,31	47,32	22,08
	10 b-values	0,29	0,12	1,15	0,31	77,15	55,27
	16 b-values	0,28	0,12	1,15	0,31	70,61	46,71

Results show that the estimated value for D remained the same for both patients and controls, independently of N_b. This is to be expected since the decrease in Nb only affected the lower b-value range (<200 s/mm^2), thus not influencing the calculation of D. However, the dependence of the estimated values for fp and D* are much larger, especially in the case of D* where the value estimated for N_b=8 is approximately half of that calculated for N_b=16.

Considering the differences between patients and controls, it is possible to say that they were very similar for the sequences with 10 and 16 b-values, however the same thing did not happen with 8 b-values, where the difference between D* of Patients and Controls is not significant, suggesting a dependence of N_b for the diagnosis of liver diseases.

3.2.2 Comparison between Controls and Patients with Steatosis

The differences in IVIM-DWI estimated parameters between controls and the sub-group of patients with Steatosis was investigated as a function of N_b. Table 3.2 shows the mean and standard deviation for each IVIM-DWI estimated parameter, for both patients with Steatosis and controls, and similarly to what was previously described, considering b-value sequences with N_b=8, 10 and 16.

Table 3.2 - Comparison between the Control group and the Patient with Pathology group, regarding IVIM-DWI parameters estimation.

		Fp		D(*10^{-3}mm^2/s)		D*(*10^{-3}mm^2/s)	
		Mean	**StdDev**	**Mean**	**StdDev**	**Mean**	**StdDev**
Patients with Steatosis	**8 b-values**	0,31	0,11	1,06	0,13	40,25	24,15
	10 b-values	0,28	0,11	1,06	0,13	73,37	39,60
	16 b-values	0,28	0,10	1,06	0,13	56,56	11,82
Controls	**8 b-values**	0,30	0,12	1,15	0,31	47,32	22,08
	10 b-values	0,29	0,12	1,15	0,31	77,15	55,27
	16 b-values	0,28	0,12	1,15	0,31	70,61	46,71

Results show that, again, the estimated value for D remained the same for both patients and controls, independently of N_b. Like in the previous section, this is to be expected since the decrease in N_b only affected the lower b-value range (<200 s/mm^2), thus not influencing the calculation of D. However, the dependence of the estimated values for fp and D* are much larger, especially in the case of D* in the Steatosis group, where the estimations were completely different depending on the number of b-values used.

Considering the differences between patients with pathologies and controls, it is possible to say that they were very similar for the sequences with 8 and 10 b-values, however the same thing didn't happen with 16 b-values, where the difference between D* of Patients with pathologies and Controls, especially for D* is much higher than the differences obtained with other N_b.

3.2.3 Evaluation of the influence of TE on IVIM-DWI parameter estimation

Here the influence of the echo time (TE) in IVIM-DWI parameter estimation is studied in-vivo for two subjects with the conventional b-value sequence. Figure 3.16 respectively shows the plots of data and model fit for TE=67ms and 80ms.

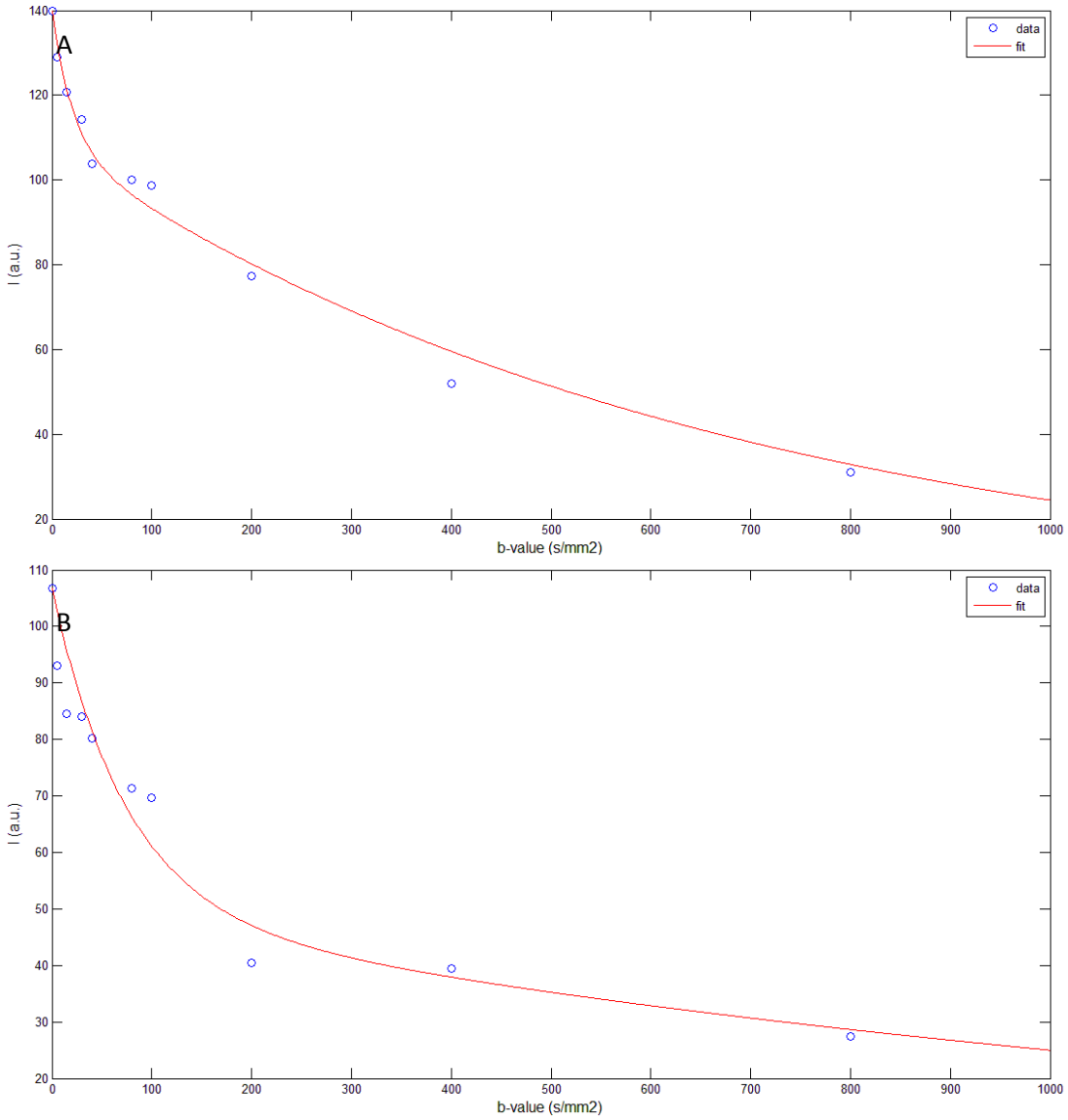

Figure 3.14 – Plot of data and model fit for TE= (A) 67ms and (B) 80ms, for subject 1.

Table 3.3 - Influence of TE in IVIM-DWI parameter estimation, for a 10 b-value conventional sequence.

Subject	TE (ms)	Fp	D(*10^{-3}mm^2/s)	D*(*10^{-3}mm^2/s)
Patient 1	**67**	0,23	1,49	45,69
	80	0,54	0,68	12,78
Patient 2	**67**	0,25	1,24	42,72
	80	0,27	1,09	156,37

Table 3.3 shows IVIM-DWI parameter estimation from data obtained with both values of TE. Results show that all the parameters tend to vary with TE, especially D* and fp which have a much larger variation. Also for higher TE, it is possible to note that some of estimations, especially D* and fp have values that are divergent from the known values for healthy liver parenchyma [26].

3.2.4 Evaluation of the conventional distribution, optimum b-value equal-weighted distribution and optimum b-value different-weighted distribution for 10 b-values

Data was acquired from six healthy volunteers (details in "Materials and Methods") with 3 b-value sequences: (A) Conventional, (B) Optimal equal-weighted, (C) Optimal different-weighted. Subsequently, IVIM parameter estimation was carried-out with the three data-sets, for each subject. Table 3.4 shows the mean and standard deviation of each IVIM-DWI parameter, for each b-value sequence and for each subject.

Table 3.4 - Influence of the type of b-value sequence used for IVIM-DWI parameter estimation.

	Fp		**D(*10^{-3}mm^2/s)**		**D*(*10^{-3}mm^2/s)**	
	Mean	**StdDev**	**Mean**	**StdDev**	**Mean**	**StdDev**
Conventional	0,42	0,10	1,46	0,56	52,85	29,61
Eq. Weights	0,45	0,13	1,33	0,26	59,41	26,83
Dif. Weights	0,40	0,17	1,51	0,42	93,37	47,17

Results show that the type of b-value sequence that is used in the acquisition has a large influence on IVIM parameter estimation, as it was previously shown with simulation studies. While fp and D remained approximately the same, independently of the b-value sequence that was used, D* is completely different when using the optimum different-weighted sequence and when compared with both conventional and optimal equal-weighted b-values sequences, having a value that is much closer to the reference for healthy liver parenchyma [26].

4. Discussion

4.1 Influence of b-value sequence

The existence of an optimum sequence for NAFLD detection and staging was studied. This subject does not have an actual consensus [21], and Zhang et al [24] pointed out that one of the most important key points of the IVIM model was actually the selection of b-values, the so called optimum b-values. This has been the object of study of few groups, with e.g. Lemke et al. [25] actually showing that the optimum b-value distribution in their study had in some cases a relative overall error two times smaller than the normally used b-value distribution.

Our simulation studies agreed with Lemke et al. [25], showing that the optimum b-value sequence considering different weighting for each IVIM-DWI parameters had the smaller error and bias of all three types of sequence. Another important point to mention is that the conventional distribution is actually better, for SNR smaller than 50, than the optimum distribution with equal weights, showing that considering equal weights for all the parameters is not a good approximation.

Our in Vivo studies were in agreement with the simulation studies since our different weighted sequence showed IVIM parameter values closer to the referenced ones for healthy liver parenchyma [26].

Thus, the b-value sequence (conventional) that is currently used in clinical practice, will lead in general to larger error and bias, thus being unreliable. In addition, the use of an optimal b-value sequence where each parameter is considered to contribute equally to the total error in the estimated parameter is inaccurate because it relies on the wrong assumption that each parameter contributes indeed equally to the total error. Therefore we can conclude that, even when using an optimum b-value sequence, considering different weights for each parameter is extremely important, since each parameter will have different contributions for the total error.

4.2 Influence of N_b

Our study is consistent with what has been referred by Patel el al. [6] and Lemke et al. [20]. Patel [6], said that the largest limitation of previous studies was the limited number of b-values used which implied an absence of differences between normal and cirrhotic livers using IVIM parameters. Lemke et al [20] also suggested that additional b-values should be used in their study for an optimal estimation of the diffusion coefficient.

In our simulation studies, especially in section 3.1.4, we could notice a great difference between using 8, 10 or 16 b-values. We noticed that bias and error behave differently, with bias remaining approximately constant for D and fp, while decreasing SNR, while larger errors were found at low SNRs. We also noticed that increasing the number of b-values that was used

to sample the signal led to a decrease in the error of each parameter. However a 10 b-value sequence had, generally, a smaller bias than a 16 b-value sequence with exception for SNR smaller than 30.We have hypothesized that these incongruities may be explained by the effect of noise in the extra b-values which would counteract the effect of having more data sampling, which lead us to think that the fact that for SNR=20, the bias for 16 b-values is smaller than for 10 b-values, may be explained by the fact that the effect of having more data sampling overcomes the effect of noise in extra b-values for low SNRs.

4.3 Influence of TE

Lemke et al [20] and Cho et al [27] observed that there was a significant increase of the fraction of perfusion with TE whereas the same type of dependence was not observed in D and D*.

Our study lacked a significant number of patients to make a truly valuable statement regarding this subject. In simulation studies, section 3.1.5, we have noticed that increasing the TE would lead to larger error and bias of all parameter estimations. This could be shown in in-vivo studies where, for longer TEs, the values of the parameter estimations deviate from the known assumed values for healthy liver parenchyma [26]. However for both subjects, fp increased with TE as in [17, 21].

This may prove the point defended for both studies which says that this fp dependence is artificially created by the large difference between the T2 relaxation time of blood and tissue, since in this situation (longer TEs) the signal drop in the lower b-value range is larger for the short (liver parenchyma) than for the long (blood) T2 species, which leads to an over estimation of fp. It is therefore extremely important that T2 relaxation effects are included in the model, thus allowing the possibility to obtain more accurate estimations, especially regarding fp.

4.4 Influence of Steatosis

There are various studies with different results considering the influence of NAFLD on IVIM-DWI parameters. However, they all agreed that D* always decreases significantly in a liver showing signs of fibrosis [5, 6, 22] or Steatosis [2, 23], leading, consequently, to a decrease in ADC. With respect to fp and D, the influence of the hepatic tissue changes in NAFLD on the variation of these parameters is still controversial [5, 22].

Our study reveals that the parameter which is more affected by changes in acquisition parameters is D*. A decrease in D is also observed, as stated by Chow et al. [5] and only a slight decrease in fp, thus in opposition to Patel et al [6] and Guiu et al [23].

However, an important thing to mention is that the differences between patients with Steatosis and controls were extremely influenced by the number of b-values that were used to

sample the data, especially regarding D* estimation. Firstly with 16 b-values, we noticed a drop of almost 20%, in D* estimation from Controls to Patients with Steatosis group, opposing to the, approximately, 5 and 15% for 10 and 8 b-values respectively. Also, the values for D* with 8 b-values in the Control group, were much smaller when compared with 10 and 16 b-values with values approximately 39% and 33% smaller, respectively. This would lead to different diagnosis depending on the number of b-values used in the acquisition, which would make this method unreliable. It is believed that this aspect needs a closer analysis, with the performance of more studies in the future.

It is important to note that the influence of each variable was always largest for D*. This allows us to hypothesize that when we are calculating an optimum b-value sequence, we are actually trying to reduce the relative error of D* since it has the largest contribution for the total propagated error.

5. Conclusion and future work

We studied the dependence of IVIM-DWI estimations on acquisition parameters. For that we proposed a new way of choosing which b-value distribution should be used to stage NAFLD. To find this distribution we firstly performed a simulation study and lastly an *in vivo* study, to confirm its effectiveness.

During our study we found that there are a huge number of factors which influence the effectiveness of each b-value sequence to estimate IVIM-DWI parameters, namely, the number of b-values, TE, T2, perfusion rate and type of b-value sequence. This implies that, depending on the type of tissue being studies, the optimum b-value sequence will always be different.

Also, we could conclude that the sequences normally used in clinical applications nowadays are not the best ones and that this should be revised since it can have a huge influence on patient diagnosis.

For future work we advise adding T2 relaxation effects to the IVIM fitting model to obtain more accurate parameter estimations. Another important conclusion is that the use of more b-values in the data acquisition does not necessarily imply smaller error and bias in parameter estimation

Finally, we noticed that in the presence of Steatosis, D and D* decreased suggesting that both molecular diffusion and perfusion change with the presence of fat in the liver, being possible to eventually use D and D* as markers of the existence of NAFLD, making IVIM-DWI a usable and, more importantly, non-invasive method to diagnose NAFLD. However its ability to distinguish pathological from healthy liver, in the context of NAFLD, is extremely dependent of the number of b-values used. This requires further research in order to determine the best methodology to find the optimum number of b-values that should be used in IVIM-DWI to diagnose NAFLD.

6. References

[1] L. A. Adams, P. Angulo, and K. D. Lindor, "Nonalcoholic fatty liver disease.," *CMAJ : Canadian Medical Association Journal*, vol. 172, no. 7, pp. 899–905, Mar. 2005.

[2] A. K. Poyraz, M. R. Onur, E. Kocakoç, and E. Oğur, "Diffusion-weighted MRI of fatty liver.," *Journal of magnetic resonance imaging : JMRI*, vol. 35, no. 5, pp. 1108–11, May 2012.

[3] J. K. Dowman, J. W. Tomlinson, and P. N. Newsome, "Systematic review: the diagnosis and staging of non-alcoholic fatty liver disease and non-alcoholic steatohepatitis.," *Alimentary pharmacology & therapeutics*, vol. 33, no. 5, pp. 525–40, Mar. 2011.

[4] P. Paschos and K. Paletas, "Non alcoholic fatty liver disease and metabolic syndrome.," *Hippokratia*, vol. 13, no. 1, pp. 9–19, Jan. 2009.

[5] A. M. Chow, D. S. Gao, S. J. Fan, Z. Qiao, F. Y. Lee, J. Yang, K. Man, and E. X. Wu, "Liver fibrosis: an intravoxel incoherent motion (IVIM) study.," *Journal of magnetic resonance imaging : JMRI*, vol. 36, no. 1, pp. 159–67, Jul. 2012.

[6] J. Patel, E. E. Sigmund, H. Rusinek, M. Oei, J. S. Babb, and B. Taouli, "Diagnosis of cirrhosis with intravoxel incoherent motion diffusion MRI and dynamic contrast-enhanced MRI alone and in combination: preliminary experience.," *Journal of magnetic resonance imaging : JMRI*, vol. 31, no. 3, pp. 589–600, Mar. 2010.

[7] M. Ziol, A. Handra-Luca, A. Kettaneh, C. Christidis, F. Mal, F. Kazemi, V. de Lédinghen, P. Marcellin, D. Dhumeaux, J.-C. Trinchet, and M. Beaugrand, "Noninvasive assessment of liver fibrosis by measurement of stiffness in patients with chronic hepatitis C.," *Hepatology (Baltimore, Md.)*, vol. 41, no. 1, pp. 48–54, Jan. 2005.

[8] P. Marcellin, M. Ziol, P. Bedossa, C. Douvin, R. Poupon, V. de Lédinghen, and M. Beaugrand, "Non-invasive assessment of liver fibrosis by stiffness measurement in patients with chronic hepatitis B.," *Liver international : official journal of the International Association for the Study of the Liver*, vol. 29, no. 2, pp. 242–7, Feb. 2009.

[9] L. Castera, X. Forns, and A. Alberti, "Non-invasive evaluation of liver fibrosis using transient elastography.," *Journal of hepatology*, vol. 48, no. 5, pp. 835–47, May 2008.

[10] R. Materne, B. E. Van Beers, a M. Smith, I. Leconte, J. Jamart, J. P. Dehoux, a Keyeux, and Y. Horsmans, "Non-invasive quantification of liver perfusion with dynamic

computed tomography and a dual-input one-compartmental model.," *Clinical science (London, England : 1979)*, vol. 99, no. 6, pp. 517–25, Dec. 2000.

[11] E. M. Haacke, R. W. Brown, M. R. Thompson, and R. Venkatesan, "Magnetic Properties of Tissues: Theory and Measurement," in in *Magnetic Resonance Imaging – Physical Principles and Sequence Design*, 1st ed., Massachusets: John Wiley & Sons, 1999, pp. 769–777.

[12] M. A. Bernstein, K. F. King, and X. J. Zhou, "Angiographic Pulse," in in *Handbook of MRI Pulse Sequences*, 1st ed., Massachusets: Elsevier Academic Press, 2004, pp. 678–698.

[13] M. A. Bernstein, K. F. King, and X. J. Zhou, "Advanced Pulse," in in *Handbook of MRI Pulse Sequences*, 1st ed., Massachusets: Elsevier Academic Press, 2004, pp. 830–856.

[14] J. Chen, M. Yin, K. J. Glaser, J. A. Talwalkar, and R. L. Ehman, "MR elastography of liver disease : State of the art," no. April, pp. 5–12, 2013.

[15] L. Huwart, C. Sempoux, E. Vicaut, N. Salameh, L. Annet, E. Danse, F. Peeters, L. C. ter Beek, J. Rahier, R. Sinkus, Y. Horsmans, and B. E. Van Beers, "Magnetic resonance elastography for the noninvasive staging of liver fibrosis.," *Gastroenterology*, vol. 135, no. 1, pp. 32–40, Jul. 2008.

[16] P. S. Hüppi and J. Dubois, "Diffusion tensor imaging of brain development.," *Seminars in fetal & neonatal medicine*, vol. 11, no. 6, pp. 489–97, Dec. 2006.

[17] H. Carr and E. Purcell, "Effects of diffusion on free precession in nuclear magnetic resonance experiments," *Physical Review*, vol. 94, no. 3, pp. 630–638, 1954.

[18] T. G. Reese, O. Heid, R. M. Weisskoff, and V. J. Wedeen, "Reduction of eddy-current-induced distortion in diffusion MRI using a twice-refocused spin echo.," *Magnetic resonance in medicine : official journal of the Society of Magnetic Resonance in Medicine / Society of Magnetic Resonance in Medicine*, vol. 49, no. 1, pp. 177–82, Jan. 2003.

[19] D. Le Bihan, E. Breton, D. Lallemand, M. Aubin, J. Vignaud, and M. Laval-Jeantet, "Separation of diffusion and perfusion in intra voxel incoherent motion MR imaging," *Radiology*, vol. 168, no. 2, pp. 497–505, 1988.

[20] A. Lemke, F. B. Laun, D. Simon, B. Stieltjes, and L. R. Schad, "An in vivo verification of the intravoxel incoherent motion effect in diffusion-weighted imaging of the abdomen.," *Magnetic resonance in medicine : official journal of the Society of Magnetic*

Resonance in Medicine / Society of Magnetic Resonance in Medicine, vol. 64, no. 6, pp. 1580–5, Dec. 2010.

[21] H. Chandarana and B. Taouli, “Diffusion and perfusion imaging of the liver.,” *European journal of radiology*, vol. 76, no. 3, pp. 348–58, Dec. 2010.

[22] A. Luciani, A. Vignaud, and M. Cavet, “Liver Cirrhosis: Intravoxel Incoherent Motion MR Imaging—Pilot Study1,” *Radiology*, vol. 249, no. 3, pp. 891–899, 2008.

[23] B. Guiu, J. Petit, V. Capitan, and S. Aho, “Intravoxel incoherent motion diffusion-weighted imaging in nonalcoholic fatty liver disease: a 3.0-T MR study,” *Radiology*, vol. 265, no. 1, pp. 96–103, 2012.

[24] J. L. Zhang, E. E. Sigmund, H. Rusinek, H. Chandarana, P. Storey, Q. Chen, and V. S. Lee, “Optimization of b-value sampling for diffusion-weighted imaging of the kidney.,” *Magnetic Resonance in Medicine*, vol. 67, no. 1, pp. 89–97, Jan. 2012.

[25] A. Lemke, B. Stieltjes, L. R. Schad, and F. B. Laun, “Toward an optimal distribution of b values for intravoxel incoherent motion imaging.,” *Magnetic Resonance Imaging*, vol. 29, no. 6, pp. 766–76, Jul. 2011.

[26] B. Guiu and J.-P. Cercueil, “Liver diffusion-weighted MR imaging: the tower of Babel?,” *European radiology*, vol. 21, no. 3, pp. 463–7, Mar. 2011.

[27] G. Y. Cho, D. K. Sodickson, and Sigmund E E, “Characterization of the TE Dependence of IVIM Biomarkers in a Flow Phantom and In Vivo,” *Proc. Intl. Soc. Mg. Reson. Med.*, vol. 161, no. IVIM, p. 3977, 2011.

7. Appendix

A. b-value optimization through the minimization of an error propagation factor

In [24], considering IVIM-DWI model equation A.1,

$$\frac{S_b}{S_0} = (1-f)\cdot\exp(-bD) + f\cdot\exp(-b(D+D^*) \quad (A.1)$$

it is noted that given a set of DWI measurements at multiple b-values b_i, parameters, fp, D*, D, can be determined in a least-squares sense by minimizing the sum of squared residue between the data and the model fit R(S_0, fp, D, D^*),

$$R(S_0, f, D, D^*) = \sum_{i=1}^{N_b} [S(b_i; S_0, f, D, D^*) - S_{b_i}]^2 \quad (A.2)$$

where N_b is the total number of b-values and S_{bi} is the signal measured at b_i. In order to minimize (2.5), partial derivatives with respect to S_0, fp, D, and D^* have to be nulled:,

$$\frac{\partial R}{\partial x(m)} = \sum_{i=1}^{N_b} \left\{ 2\cdot\left[S(b_i, x) - S_{b_i}\right]\cdot\frac{\partial S(b_i, x)}{\partial x(m)} \right\} = 0, \quad m = 1,2,3,4 \ (A.3)$$

where x(m) (m = 1, 2, 3, 4) represent S_0, fp, D, and D^*, respectively. By the Taylor's theorem, in the limit of increasing SNR, the term in square brackets of the last equation can be approximated to:

$$\sum_{n=1}^{4} \left(\delta x(n) \frac{\partial S(b_i, x)}{\partial x(n)} \right) \ (A.4)$$

Where δx is the column vector of estimation errors for each parameter. Replacing this approximation in the first equation we get,

$$\sum_{i=1}^{N_b} \left\{ \left[\sum_{n=1}^{4} \left(\delta x(n) \frac{\partial S(b_i, x)}{\partial x(n)} \right) - \varepsilon(i) \right] \cdot \frac{\partial S(b_i, x)}{\partial x(m)} \right\} = 0, \quad m = 1,2,3,4\,; (A.5)$$

Where Ɛ is the noise in the measured signals, the equation, if rearranged and expressed in matrix form, can be re-written as:

$$A\cdot\delta x = B \ (A.6)$$

Where B(m)= $\sum_{i=1}^{N_b}\left(\varepsilon(i)\cdot\frac{\partial S(b_i,x)}{\partial x(m)}\right)$, A=$J^T$J and J is the Jacobian matrix of S(x). The variance of model parameters, assuming the identical distribution and independency of the signal noise, can be obtain as,

$$[\delta x(n)]^2=\left[\delta^2\sum_{m=1}^{4}\sum_{p=1}^{4}A^{-1}(n,m)\cdot A^{-1}(n,p)\times\sum_{i=1}^{N_b}\left(\frac{\partial S(b_i,x)}{\partial x(m)}\cdot\frac{\partial S(b_i,x)}{\partial x(p)}\right)\right]\ (A.7)$$

Where δ^2 is the variance of noise. An error propagation factor ξ is defined as the ratio of the relative error in a model parameter to the relative input noise δ/S_0,

$$\xi(n)=\frac{\delta x(n)/x(n)}{\delta/S_0}=$$

$$=\frac{S_0}{x(n)}\sqrt{\sum_{m=1}^{4}\sum_{p=1}^{4}\left[A^{-1}(n,m)\cdot A^{-1}(n,p)\cdot\sum_{i=1}^{N_b}\left(\frac{\partial S(b_i,x)}{\partial x(m)}\cdot\frac{\partial S(b_i,x)}{\partial x(p)}\right)\right]}\ (A.8)$$

The partial derivatives are

$$\frac{\partial S}{\partial S_0}=(1-F_P)e^{-b\cdot D_T}+F_P e^{-b\cdot D_P}\quad(A.9)$$

$$\frac{\partial S}{\partial S_P}=S_0[e^{-b\cdot D_P}-e^{-b\cdot D_T}]\qquad(A.10)$$

$$\frac{\partial S}{\partial D_T}=-S_0(1-F_P)e^{-b\cdot D_T}b\qquad(A.11)$$

$$\frac{\partial S}{\partial D_P}=-S_0F_P e^{-b\cdot D_P}b\qquad(A.12)$$

Thus, if we keep each parameter over their expected ranges for the type of tissue we are interested in, we can obtain the error propagation factor for each on of them, and adjust the b values in order to minimize this error. Since we are normally interested in differentiating tissues, a generalization of equation 2.6 can be re-written as:

$$\bar{\xi}=\int_{D^{min}}^{D^{max}}\int_{D^{*min}}^{D^{*max}}\int_{f^{min}}^{f^{max}}(W_f\,\xi_f+W_{D^*}\xi_{D^*}+W_D\xi_D)df dD^* dD\ (A.10)$$

where W_x are positive weighting factor specified by the user and X^{max} and X^{min} are the expected range values of each parameter.

B. Simulation Studies additional images

B.1

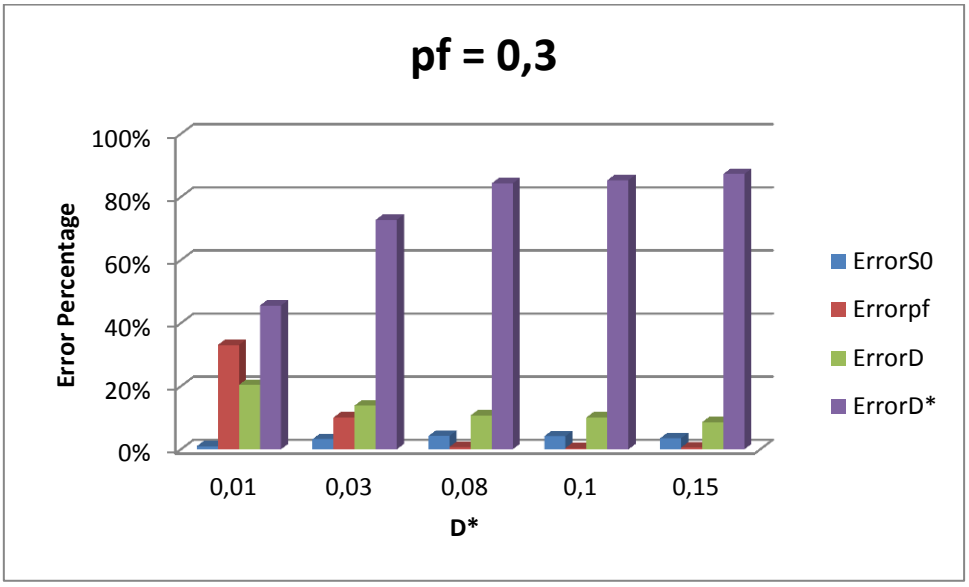

Figure B.1 - Study of influence of D* in parameters relative propagated error for a fp=0.3, considering 10 b-values.